Quantum Effects in One-Dimensional Optical Flat-Band Lattices

Markku Hyrkäs

Master's Thesis
University of Jyväskylä, Department of Physics
November 14, 2011
Supervisor: Matti J. Manninen

Abstract

I numerically simulated one-dimensional lattice systems describable by the Hubbard-model and containing a flat-band. I studied the manner in which particles initially held in place by a parabolic confinement potential are dispersed across the lattice after the potential is removed. I also studied currents flowing within one-dimensional Hubbard-rings. In both of these cases I observed that the flat dispersion relation of the flat-band manifests itself as the immobility of the particles occupying it. Particles occupying flat-band states do not disperse even after the removal of any external confinement, neither do they contribute to a current within a ring.

Tiivistelmä

Optiset hilat ovat periodisia sähköisiä potentiaaleja, jotka muodostuvat vastakkain asetettujen lasersäteiden interferoidessa. Tällaisen potentiaalin minimikohtiin voidaan kaapata ultrakylmiä neutraaleja atomeja, jolloin muodostuu eräänlainen keinotekoinen kidehila. Optiset hilat ovat monella tapaa analogisia todellisten kiteisten materiaalien hilojen kanssa, mutta ne ovat merkittävästi yksinkertaisempia mallintaa ja havainnoida, ja lisäksi niiden parametrit ovat tarkasti säädettävissä. Optiset hilat ovatkin monikäyttöisiä ja tehokkaita kokeellisia työkaluja, ja sen jälkeen kun niiden rakentaminen tuli mahdolliseksi laser-jäähdytysmenetelmien kehityksen seuraksena pari vuosikymmentä sitten, ne ovat löytäneet sovelluksia monilla eri fysiikan aloilla aina kiinteän aineen fysiikasta kvantti-informaatioteoriaan.

Yksi optisten hilojen mielenkiintoinen piirre on se, että monessa tapauksessa niitä on mahdollista mallintaa suurella tarkkuudella käyttäen hyvin tunnettuja ja suhteellisen yksinkertaisia Hubbard-tyyppisiä Hamiltonin operaattoreita. Tässä työssä keskityin yksiulotteisiin optisiin hiloihin, joita mallinsin käyttäen yksiulotteista Hubbardin mallia. Tutkimiani hiloja yhdisti se, että niillä oli vähintään yksi energiavyö, jonka dispersio oli vakio kaikilla aaltoluvun arvoilla. Tälläisellä dispersiottomalla energiavyöllä sijaitsevalla hiukkasella on ääretön efektiivinen massa, ja vastaavasti sen ryhmänopeus on nolla, eikä se täten liiku hilassa lainkaan.

Suoritin numeerisia simulaatioita kahdessa erilaisessa Hubbard-hilassa (katso luku 3). Ensimmäisessä osassa tutkin kuinka johonkin hilan osaan keskittynyt hiukkasrypäs leviää ajan kuluessa. Muodostin ensin alkutilan laskemalla perustilan systeemille johon sisältyi ulkoinen parabolinen keskittävä potentiaali. Laskin sitten tämän tilan aikakehityksen kun ulkoinen potentiaali oli poistettu. Toisessa osassa tutkin virtaa hiloista muodostetuissa renkaissa, ja erityisesti sitä miten virta muuttui hiukkaslukumäärän funktiona. Molemmissa tapauksissa kiinnitin huomiota siihen miten dispersiottomien energiavöiden miehitys vaikutti tuloksiini. Havaitsin että tällaisilla vöillä olevat hiukkaset eivät hajaannu vaikka ulkoista keskittävää potentiaalia ei olisi, eivätkä ne myöskään vaikuta renkaassa kulkevaan virtaan.

Contents

Chapter 1

Introduction

Artificial crystal structures of neutral atoms held in periodic optical potentials are a relatively new and a highly versatile experimental tool which offers many intriguing possibilities for studying quantum many-body systems in precisely controlled environments (See review [7]). After the realization of these optical lattices was made possible some two decades ago by advances in laser cooling technology, they have been utilized widely in diverse fields ranging from solid-state physics to quantum information theory.

One interesting aspect of these systems is that in many cases they can be modeled to a very high accuracy using the well known and relatively simple Hubbard-type Hamiltonians. In this work I will concentrate on one-dimensional optical lattices described by a one-dimensional Hubbard model. I'll study a few different types of these Hubbard-chains, which all share the property of containing an energy band with a flat dispersion for all values of the wave number. These so-called flat-bands are characterized by the immobility of the particles occupying them.

I perform numerical simulations concentrating on two types of Hubbard-chains: the sawtooth-chain and the diamond-chain (see chapter 3). In the first part I will study the manner in which a concentrated bunch of particles spreads out within the chains. I first obtain the initial bunched up state by computing the ground state of a system with an external parabolic potential overlaid across the lattice. I then compute the time evolution of this state when the external potential has been switched off. In the second part I study currents flowing within rings formed from the chains, and especially how these currents depend on the number of particles in the ring. In both of these cases I will attempt to find manifestations of the immobility of the flat-band particles.

Chapter 2

Theory

2.1 Optical Lattice

Optical lattices are periodic electric potentials created by interference of counter-propagating laser beams. They can be used to capture ultra-cold atomic gases consisting of neutral atoms, creating periodic many-body systems for use in experiments. The idea of using standing light waves for trapping of atoms was first put forward by V.S. Letokhov in 1968 [1], and the first optical lattice was build in 1987 [2]. In this first experiment cesium atoms were used, but afterwards many other species of atomic gases have been inserted into optical lattices.

A System consisting of atoms in an optical lattice is in many ways analogous to a system of electrons in a crystal lattice. However, compared to corresponding condensed-matter systems, optical lattices are dramatically simpler to model. They have no defects, and they do not support phononic excitations. They are also highly tunable, and easy to observe. This makes them extremely useful as model systems for studying theoretical concepts of condensed-matter physics [3], as well as fundamental problems of many-body quantum mechanics. Optical lattices can also be used to trap and study Bose-Einstein condensates [4, 6], and the extraordinary control allowed by them has given them applications in the field of quantum information processing [5, 3].

An optical lattice is build by arranging laser beams in such a way, that their interference creates a periodic standing wave. In such case the average electric field intensity becomes periodic in space, and consequently the atoms will receive a different induced dipole moment depending on their location. The interaction between this dipole moment and the electric field results in a force, which focuses the particles either on the maxima, or the minima, of

the electric field. This force is known as the dipole force, and it is explained in greater detail in the section 2.1.1.

In practice an optical lattice is never completely homogeneous, since the intensity of a laser beam is not constant. The intensity drops towards the edges of the beam, which results in a confining potential superimposed over the lattice. This confinement is typically relatively weak, having an oscillatory frequency two to three orders of magnitude lower than that of the potential wells of the lattice [7]. In this work I'll assume its effect to be negligible, and will not take it into account.

There exists an alternative way to build an optical lattice, where the electric field intensity remains constant across space, and instead the polarization of the standing wave changes periodically between linear and cylindrical. In this kind of lattice an effect known as Sisyphus cooling takes place, which can cool the atoms down to temperatures below a microkelvin [6, p. 84]. In the following discussion, however, these types of constructions will not come up.

2.1.1 The Dipole Force

An atom moving in an electric field will receive an induced dipole moment, and have its energy levels shifted by the Stark effect. In the so-called dipole approximation, in which the electric field is assumed to be constant on atom sized length scales, the Hamiltonian describing the interaction between the atom and the electric field can be written as

$$\hat{H}_d = -\mathbf{d} \cdot \mathcal{E},$$

where $d = -e\sum_i \mathbf{r}_i$ is the dipole moment operator, $\mathbf{r}_i$ are the positions of the electrons with respect to the nucleus and $\mathcal{E}$ is the electric field vector. The electric field vector can be expressed in the form

$$\mathcal{E}(\mathbf{r}, t) = \mathcal{E}_{+\omega} e^{-i\omega t} + \mathcal{E}_{-\omega} e^{i\omega t},$$

where choosing $\mathcal{E}_{-\omega} = \mathcal{E}^*_{+\omega}$ ensures that $\mathcal{E}$ is real.

In the lowest order the interaction between the electric field and an atom can happen in two ways. Either the atom first absorbs an photon, and then emits it, or vice versa (see figure 2.1). Before and after the process the atom is in its ground state g, and between the interactions in an excited state e. These processes cause the ground state energy of the atom to shift. The effect is known as AC Stark-effect, because it is analogous to the Stark-effect for time independent electric fields. Based on the graphs in figure 2.1, one

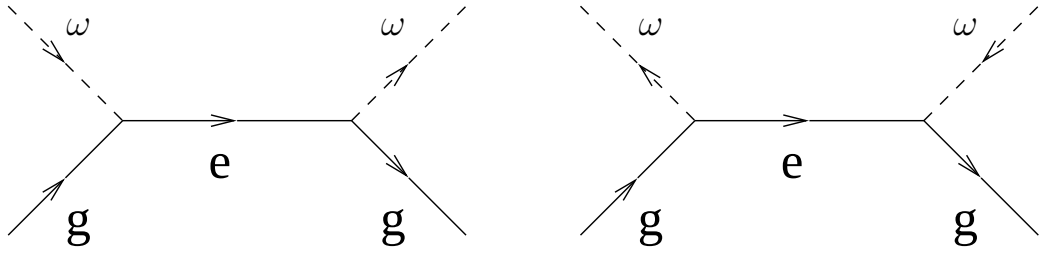

Figure 2.1: Interaction between an atom on its ground state, and a time dependent electric field. Solid line depicts the atom, and dashed line a photon.

can write down a perturbative expression for the energy shift. Vertices of the graphs give transition amplitudes of the form

$$-\langle \text{final state}|\mathbf{d}\cdot\mathcal{E}_{\pm\omega}|\text{initial state}\rangle,$$

where + corresponds to photon emission, and − to photon absorption. The internal propagator between the vertices is

$$\frac{1}{(E_g \mp \hbar\omega) - E_e},$$

where $\hbar\omega$ is the energy of the photon, and − corresponds to an emitted and + to an absorbed photon. Multiplying these terms together, and summing over the graphs and all possible excited states, one gets for the ground state energy shift an expression

$$\begin{aligned}\triangle E_g &= \sum_e \langle g|\mathbf{d}\cdot\mathcal{E}_{+\omega}|e\rangle \frac{1}{E_g - E_e + \hbar\omega}\langle e|\mathbf{d}\cdot\mathcal{E}_{-\omega}|g\rangle \\ &+ \sum_e \langle g|\mathbf{d}\cdot\mathcal{E}_{-\omega}|e\rangle \frac{1}{E_g - E_e - \hbar\omega}\langle e|\mathbf{d}\cdot\mathcal{E}_{+\omega}|g\rangle \\ &= \sum_e |\langle e|\mathbf{d}\cdot\hat{\mathbf{e}}|g\rangle|^2 \left(\frac{1}{E_g - E_e + \hbar\omega} + \frac{1}{E_g - E_e - \hbar\omega}\right)|\mathcal{E}_\omega|^2. \qquad (2.1)\end{aligned}$$

In the case of a time independent electric field, the polarizability α of an atom is defined as the factor between the electric field intensity and the expectation value of the dipole moment operator

$$\langle \mathbf{d}\rangle = \alpha\mathcal{E}.$$

The energy of the dipole in the dipole approximation is $E = -\langle \mathbf{d}\rangle\cdot\mathcal{E}$. A change in the electric field then results in an energy shift of

$$dE = -\langle \mathbf{d}\rangle\cdot d\mathcal{E} = -\alpha\mathcal{E}d\mathcal{E},$$

and the total energy shift when integrating over the electric field from zero to $\mathcal{E}$ is

$$E - E_0 = \triangle E = -\frac{1}{2}\alpha\mathcal{E}^2. \tag{2.2}$$

In the case of a time dependent electric field, one can use an expression analogous to (2.2)

$$\triangle E = -\frac{1}{2}\alpha(\omega) < \mathcal{E}(\mathbf{r},t)^2 >_t,$$

where $\alpha(\omega)$ is the polarizability, which now depends on the laser field frequency, and $< ... >_t$ denotes a time average. This form is achieved, when one inserts into equation (2.1)

$$|\mathcal{E}_\omega|^2 = \frac{1}{2} < \mathcal{E}(\mathbf{r},t)^2 >_t$$

and defines

$$\alpha(\omega) = \sum_e |\langle e|\mathbf{d}\cdot\hat{\mathbf{e}}|g\rangle|^2 \left(\frac{1}{E_e - E_g + \hbar\omega} + \frac{1}{E_e - E_g - \hbar\omega}\right). \tag{2.3}$$

From equation (2.3) one sees, that when the radiation frequency matches with an atomic resonance, that is $(E_e - E_g)/\hbar = \omega$, the term $1/(E_e - E_g - \hbar\omega)$ diverges. Therefore when close to the resonant frequency, a good approximation for the polarizability can be achieved by considering only this divergent term. Equation (2.3) then simplifies to the form

$$\alpha(\omega) \approx \frac{|\langle e|\mathbf{d}\cdot\hat{\mathbf{e}}|g\rangle|^2}{E_e - E_g - \hbar\omega}.$$

The divergence in the polarizability is a consequence of ignoring the finite lifetime of the excited state. Let the transition frequency from the excited state e to the ground state g be Γ_e. The amplitude for the excited state must then contain a factor $\exp(-\Gamma_e t/2)$ describing the exponential decay. Because the time dependence of an energy eigenstate is described by a factor $\exp(-iE_e t/\hbar)$, the finite lifetime can be handily accounted for by writing the energy in the form

$$E_e' = E_e - i\hbar\Gamma_e/2,$$

which gives

$$e^{-iE_e' t/\hbar} = e^{-i(E_e - i\hbar\Gamma_e/2t)/\hbar} = e^{-iE_e t/\hbar}\cdot e^{-\Gamma_e t/2}.$$

Equation for the polarizability (2.3) then takes the form

$$\alpha(\omega) \approx \frac{|\langle e|\mathbf{d}\cdot\hat{\mathbf{e}}|g\rangle|^2}{E_e - i\hbar\Gamma_e/2 - E_g - \hbar\omega},$$

and the energy shift of the ground state is

$$\triangle E_g = -\frac{1}{2} Re(\alpha(\omega)) < \mathcal{E}(\mathbf{r},t)^2 >_t, \tag{2.4}$$

where

$$Re(\alpha(\omega)) \approx \frac{(E_e - E_g - \hbar\omega)|\langle e|\mathbf{d}\cdot\hat{\mathbf{e}}|g\rangle|^2}{(E_e - E_g - \hbar\omega)^2 + (\hbar\Gamma_e/2)^2}. \tag{2.5}$$

The energy shift acts as an effective external potential, which exerts to the atom a force

$$\mathbf{F}_d = -\nabla V(\mathbf{r}) = \frac{1}{2} Re(\alpha(\omega))\nabla < \mathcal{E}(\mathbf{r},t)^2 >_t . \tag{2.6}$$

The difference between the laser frequency and the atomic transition frequency $\delta = \omega - (E_e - E_g)/\hbar$ is often called the detuning. From the equation for the polarizability (2.5) it can be seen, that if $\delta > 0$ (blue detuning) the force points towards the minima of the electric field, and if $\delta < 0$ (red detuning), it points towards the maxima. Furthermore, the strength of the dipole force (2.6) is dependent on the value of the detuning. There are thus two ways to adjust the depth of the optical lattice potential: changing the detuning, or changing the laser intensity. In an actual experiment the laser frequency has to be set sufficiently far from any atomic transition to avoid the gas being heated by the absorption of photons from the beam.

2.1.2 Constructing an Optical Lattice

The equation (2.4) gives the potential felt by an atom moving in an electric field

$$V(\mathbf{r}) = -\frac{1}{2} Re(\alpha(\omega)) < \mathcal{E}(\mathbf{r},t)^2 >_t,$$

where $Re(\alpha(\omega))$ is the real part of the polarizability (equation 2.5), and $< \mathcal{E}(\mathbf{r},t)^2 >_t$ is the time average of the square of the electric field. The potential landscape is thus determined by the average electric field intensity. If it varies in space, there will be a force exerted on the atom.

Two lasers, having the same frequency and being linearly polarized along the same plane, placed oppositely against each other, will generate an electric field of the form

$$\mathcal{E} = \mathcal{E}_0 cos(qx - \omega t) + \mathcal{E}_0 cos(-qx - \omega t) = 2\mathcal{E}_0 cos(qx) cos(\omega t).$$

The time average of the square of this field is

$$< \mathcal{E}^2 >_t = 4\mathcal{E}_0^2 cos^2(qx) \frac{1}{2\pi/\omega} \int_0^{2\pi/\omega} cos^2(\omega t) dt = 2\mathcal{E}_0^2 cos^2(qx) = \mathcal{E}_0^2(1 + cos(2qx)).$$

The result is then a one-dimensional periodic electric potential, i.e. an optical lattice. If two or three of this kind of laser pairs, with mutually orthogonal polarization vectors, are set up to cross in the same spot, the result is respectively a two- or three-dimensional cubic lattice.

By arranging the lasers in a suitable manner, almost any kind of periodic potential can be realized. Changing the angle of incidence of a laser pair changes the lattice constant of the resulting lattice. If the laser frequencies differ slightly the result is a moving lattice, and by changing the frequency difference over time one can make the lattice accelerate. The depth of the potential wells can be changed by adjusting the intensity of the lasers. Even the strength of the interaction between the atoms can be adjusted, through an effect known as the Feshbach resonance (see [9] for a review on the subject). An optical lattice is then an extremely versatile and a highly adjustable experimental tool.

2.2 Particles in a Lattice

Building a quantum mechanical description of a particle in a lattice starts with the question: what do the energy eigenfunctions look like in an infinite periodic potential? Clearly in the limit of a very weak lattice potential, the states should resemble those of a free particle, i.e. plane waves. Conversely in the limit of an extremely strong potential, when the potential wells on the lattice sites become essentially separated, the eigenstates should become discrete bound states resembling those of a harmonic oscillator. One would expect then that for an average potential strength the states would share properties from both of these extremes, being perhaps both k-dependent as the plane waves, and discrete as the harmonic states.

This is in fact the case. The form of an energy eigenfunction in an infinite periodic potential was first given by Felix Bloch in 1928 [8], and these functions became known as Bloch waves. A Bloch wave function is a modulated plane wave, the modulating function having the periodicity of the underlying potential. It can be written as

$$\varphi_{\alpha\mathbf{k}}(\mathbf{x}) = e^{i\mathbf{k}\cdot\mathbf{x}} u_{\alpha\mathbf{k}}(\mathbf{x}), \tag{2.7}$$

where $\mathbf{k}$ is called the crystal momentum and $u_{\alpha\mathbf{k}}(\mathbf{x}+\mathbf{R}) = u_{\alpha\mathbf{k}}(\mathbf{x})$ for any lattice vector $\mathbf{R}$ (for derivation see [10, p. 134]). The function $u_{\alpha\mathbf{k}}(\mathbf{x})$ can be thought to be formed from the wave functions of the bound states, which broaden and mix as the potential strength is lowered. We use the subscript α to denote the discrete bound state the Bloch wave derives from.

There is a different wave function, and thus energy, corresponding to each value of α. Each of these wave functions, as well as energies, is also a function of $\mathbf{k}$. In the context of a lattice α is called the band index, and the corresponding energies $E_\alpha(\mathbf{k})$ are called the energy bands.

The Bloch wave is periodic in the reciprocal lattice [11, p. 131], it can therefore be written as a Fourier expansion

$$\varphi_{\alpha\mathbf{k}}(\mathbf{x}) = \sum_i \phi_\alpha(\mathbf{R}_i, \mathbf{x}) e^{i\mathbf{k}\cdot\mathbf{R}_i}, \tag{2.8}$$

where the coefficients $\phi_\alpha(\mathbf{R}_i, x)$ are given by

$$\phi_\alpha(\mathbf{R}_i, \mathbf{x}) = \frac{1}{L}\sum_{\mathbf{k}} \varphi_{\alpha\mathbf{k}}(\mathbf{x}) e^{-i\mathbf{k}\cdot\mathbf{R}_i}, \tag{2.9}$$

where L is the number of sites in the lattice.

It is easy to show that Bloch functions fulfill

$$\varphi_{\alpha\mathbf{k}}(\mathbf{x}+\mathbf{R}_i) = e^{i\mathbf{k}\cdot\mathbf{R}_i}\varphi_{\alpha\mathbf{k}}(\mathbf{x}). \tag{2.10}$$

By plugging (2.10) into (2.9) we find out that

$$\phi_\alpha(\mathbf{R}_i, \mathbf{x}) = \frac{1}{L}\sum_{\mathbf{k}} \varphi_{\alpha\mathbf{k}}(\mathbf{x}-\mathbf{R}_i) e^{i\mathbf{k}\cdot\mathbf{R}_i} e^{-i\mathbf{k}\cdot\mathbf{R}_i} = \frac{1}{L}\sum_{\mathbf{k}} \varphi_{\alpha\mathbf{k}}(\mathbf{x}-\mathbf{R}_i) = \phi_\alpha(\mathbf{x}-\mathbf{R}_i), \tag{2.11}$$

i.e. that ϕ's depend on $\mathbf{x}$ and $\mathbf{R}_i$ only through their difference.

The $\phi_\alpha(\mathbf{x}-\mathbf{R}_i)$'s are called Wannier functions. They are wave functions that are concentrated around the sites of the lattice, in effect wave packets formed out of the Bloch waves. It is seen from (2.8) that every Bloch wave can be written as a linear combination of the Wannier functions. This, together with their orthogonality, means that the Wannier functions form an alternate complete orthogonal basis for the periodic system. This basis will later prove to be very useful when we consider the Hubbard model.

In the case of a unit cell that contains more than a single lattice site the Bloch wave is formed in a similar manner, but instead of a single Wannier function, we use a linear combination of them in the form

$$\Phi_\alpha(\mathbf{x}-\mathbf{R}_i) = \sum_n^{N_s} c_{n\alpha}\phi_\alpha(\mathbf{x}-\mathbf{R}_i-\mathbf{a}_n).$$

where N_s is the number of sites in the unit cell and $\mathbf{a}_n$ are the basis vectors. The Bloch wave is then expressed similarly to (2.8) as

$$\varphi_{\alpha\mathbf{k}}(\mathbf{x}) = \sum_i \Phi_\alpha(\mathbf{x}-\mathbf{R}_i) e^{i\mathbf{k}\cdot\mathbf{R}_i}. \tag{2.12}$$

2.2.1 The Hubbard Model

The Hubbard model is an approximate model for describing interacting particles in a periodic lattice. It was originally introduced by John Hubbard in 1963 to model electrons in a solid [12], but can be used equally well to model other fermions, as well as bosons, in which case it is known as the Bose-Hubbard model. The model consists of two main components:

1. an ability of the particles to hop between neighboring lattice sites
2. an on-site interaction potential, felt by particles occupying the same lattice site.

Accordingly the parameters defining a Hubbard model consist of an interaction term, which gives the strength of the on-site repulsion, and a collection of hopping terms, which give the likelihood of a particle hopping between any two lattice sites.

Despite its apparent simplicity, finding the exact solution of the Hubbard model has proved an enormously difficult task. After almost half a century of research, it has only been managed in the one-dimensional case (in 1968 by E.H. Lieb and F.Y. Wu, using the so-called Bethe ansatz [13]). The model can, however, be studied using a variety of numerical methods, and this reveals many interesting properties that make a Hubbard system qualitatively different from a non-interacting tight-binding system. The most important of these is probably the appearance of a phase transition into a Mott insulating state.

The Mott transition happens in a lattice that contains approximately one particle per lattice site, when the ratio between the parameters describing the strength of the interaction and the amount of hopping between sites reaches a certain threshold. The particles spread out uniformly across the lattice with one particle in each site, and the system becomes jammed, with each particle preventing its neighbors from changing site. This state resembles an insulator, even though there is no band gap. The interplay between these two competing aspects, hopping and the interaction, is what gives the Hubbard model many of its interesting properties.

The Hubbard model turns out to manifest a surprisingly rich array of phenomena. Even though it is based on several hugely simplifying approximations, and consequently cannot really accurately describe any real materials, it still manages to capture many of the essential features of more general interacting many-body systems. It has been widely used, and proved very powerful, as a model system providing qualitative insight into many phenomena of solid state physics. It is even believed that the 2D Hubbard model

may contain important information regarding the mechanisms behind high temperature superconductivity [14].

In the context of optical lattices, however, the Hubbard model takes on a rather different role. A system consisting of cold atomic gas held in an optical lattice resembles in many ways the case of electrons in a crystal lattice. The atoms in it interact with each other, and tunnel from site to site, in a similar manner. However, due to the simplicity of optical lattices, it turns out that many of the severe approximations behind the Hubbard model are no longer needed. In fact it has been shown that an optical lattice can be constructed in such a way, that it realizes the Hubbard model with very high accuracy [15]. Furthermore, in an optical lattice the parameters of the model can be adjusted freely, for example to induce a phase transition.

The situation reverses in a way. Instead of using the Hubbard model to understand the optical lattice system, one can use the system to study the properties of the model. The optical lattice works as a kind of primitive quantum computer, in which one can run simulations of quantum mechanical models much faster than on any conventional machine. Due to the adjustability of an optical lattice this computer can be set up to simulate a large array of Hamiltonians, including Hubbard models with different parameters and several types of spin models (see [3] for a review on the subject).

The Hubbard Hamiltonian in a lattice

Let us now derive the Hubbard model Hamiltonian starting from a more general many-body Hamiltonian. The Hamiltonian describing N interacting particles in a static periodic potential is

$$\begin{aligned}\hat{H} &= \sum_{i=1}^{N}\left(\frac{\hat{\mathbf{p}}_i^2}{2m} + V_L(\mathbf{x}_i)\right) + \sum_{1\le i<j\le N} V_I(\mathbf{x}_i - \mathbf{x}_j) \\ &= \sum_{i=1}^{N}\hat{h}(\mathbf{x}_i, \mathbf{p}_i) + \sum_{1\le i<j\le N} V_I(\mathbf{x}_i - \mathbf{x}_j),\end{aligned} \tag{2.13}$$

where V_L is the periodic lattice potential, V_I is the interaction potential between the particles, and

$$\hat{h} = \frac{\hat{\mathbf{p}}_i^2}{2m} + V_L(\mathbf{x}_i) \tag{2.14}$$

is the one-particle Hamiltonian. The assumption has been made here, that the underlying periodic potential V_L does not vary over time. In the case of an optical lattice, this is clearly valid. In an actual solid it may not be,

due to the possibility of phonon excitations in non-zero temperatures. Still it can be justified in many cases, through the so-called Born-Oppenheimer approximation [16, p. 175].

First we'll want to second-quantize the Hamiltonian in some basis of one-particle states. One such basis is formed by the energy eigenstates, which in an infinite periodic potential are the Bloch functions $\varphi_{\alpha k}(\mathbf{x})$ (see equation (2.7)). We'll mark the corresponding energies by $E_{\alpha\mathbf{k}}$, so that

$$\hat{h}\varphi_{\alpha\mathbf{k}}(\mathbf{x}) = E_{\alpha\mathbf{k}}\varphi_{\alpha\mathbf{k}}(\mathbf{x}).$$

A more suitable basis for our needs, however, is the basis formed by the site-centered Wannier functions $\phi_{\alpha i}(\mathbf{x})$ (see (2.9)). We'll assume that the Wannier states are highly localized, i.e. that they are almost entirely contained within their assigned lattice sites, with only minimal overlap with the wave functions on neighboring sites. While problematic for real solids, in optical lattices this assumption is in many cases valid. The range of the Wannier functions is generally related to the size of the band gap, with a larger gap leading to a shorter range [17]. In optical lattices the width of the band gap can be adjusted by changing the depth of the potential wells, which effectively controls the spread of these wave functions.

The localized Wannier basis is important, because it facilitates the transition from the conceptual description of the Hubbard model into its mathematical formulation in terms of quantum mechanics. The Hubbard model is expressed from the viewpoint of a particle sitting on a certain site of the lattice. We can now say what this actually means: that the particle is occupying the Wannier state corresponding to that lattice site.

Let us now introduce the creation and annihilation operators

$$\hat{a}^\dagger_{\alpha i,s}, \qquad \hat{a}_{\alpha i,s},$$

which respectively create and annihilate a particle with spin s from the Wannier state on band α and site i. From these one can construct the field operators

$$\hat{\Psi}^\dagger_s(\mathbf{x}) = \sum_{\alpha i} \phi^*_\alpha(\mathbf{x} - \mathbf{R}_i)\hat{a}^\dagger_{\alpha i,s}, \qquad \hat{\Psi}_s(\mathbf{x}) = \sum_{\alpha i} \phi_\alpha(\mathbf{x} - \mathbf{R}_i)\hat{a}_{\alpha i,s}, \qquad (2.15)$$

which create or destroy a particle with spin s on location $\mathbf{x}$.

Using the field operators we can now express the Hamiltonian 2.13 in its

second quantized form [18, p. 221]

$$\hat{H} = \sum_{s=\uparrow,\downarrow} \int dx^3 \hat{\Psi}_s^\dagger(\mathbf{x}) H_i \hat{\Psi}_s(\mathbf{x}) + \frac{1}{2} \sum_{s,s'=\uparrow,\downarrow} \int dx^3 dy^3 \hat{\Psi}_s^\dagger(\mathbf{x}) \hat{\Psi}_{s'}^\dagger(\mathbf{y}) V_I(x,y) \hat{\Psi}_{s'}(\mathbf{y}) \hat{\Psi}_s(\mathbf{x}). \tag{2.16}$$

Inserting the definitions (2.15) into (2.16) we get

$$\hat{H} = \sum_{\alpha,i,j,s} t_{ij}^\alpha \hat{a}_{\alpha i,s}^\dagger \hat{a}_{\alpha j,s'} + \frac{1}{2} \sum_{\substack{\alpha,\beta,\gamma,\delta \\ i,j,k,l}} \sum_{s,s'} U_{ijkl}^{\alpha\beta\gamma\delta} \hat{a}_{\alpha i,s}^\dagger \hat{a}_{\beta j,s'}^\dagger \hat{a}_{\gamma k,s'} \hat{a}_{\delta l,s}, \tag{2.17}$$

where

$$t_{ij}^\alpha = \int dx^3 \phi_\alpha^*(\mathbf{x} - \mathbf{R}_i) \hat{h}(\mathbf{x}, \mathbf{p}) \phi_\alpha(\mathbf{x} - \mathbf{R}_j) \tag{2.18}$$

$$= \frac{1}{N_s^2} \sum_{\mathbf{k}} E_{\alpha\mathbf{k}} e^{i\mathbf{k}\cdot(\mathbf{R}_i - \mathbf{R}_j)} \tag{2.19}$$

and

$$U_{ijkl}^{\alpha\beta\gamma\delta} = \int dx^3 dy^3 \phi_\alpha^*(\mathbf{x}-\mathbf{R}_i) \phi_\beta^*(\mathbf{y}-\mathbf{R}_j) V_I(\mathbf{x},\mathbf{y}) \phi_\gamma(\mathbf{y}-\mathbf{R}_k) \phi_\delta(\mathbf{x}-\mathbf{R}_l). \tag{2.20}$$

I am not in this work concerned with the exact form of the Wannier functions, or of the potentials, and will regard t's and U's simply as parameters of the theory.

It is easy now to decipher the meaning of the terms in the Hamiltonian (2.17). The first term annihilates a particle in a lattice site, and creates one in another. It thus describes the tunneling of a single particle to another location. Strength of the tunneling between sites i and j is given by the matrix element t_{ij}^α. These elements are called 'hopping terms'. The second term of the Hamiltonian causes two particles to be annihilated, and in turn creates two new particles. It thus describes a scattering process between two particles, the strength of which is determined by the corresponding U-term.

The hopping terms are transition amplitudes between different Wannier states, and their magnitude depends on the amount of overlap between the corresponding wave functions. We assumed earlier, that the Wannier functions are highly localized. We can thus conclude that the overlap will only

be significant between sites that are immediately next to each other. We can then set $t = 0$ for all the other values of i and j, so that tunneling will only happen between neighboring sites. This is known as the tight-binding approximation.

Turning now to the potential term U, we would like it to be very small for particles that are not in the same lattice site. However, in addition to the dependence on wave function overlaps, it also depends on the strength of the interaction $V_I(\mathbf{x}, \mathbf{y})$ between the particles. In the case of a real solid, this interaction is the Coulomb interaction, which is by no means on-site. The assumption can be partly justified by appealing to the background of oppositely charged nuclei, which screens the interactions on long distances [19, p. 2]. In the case of optical lattices, however, the situation is again much simpler. The atoms loaded into an optical lattice are neutral, and the only long range interactions between them are caused by small Van der Waals type forces, which one can generally safely ignore. On the other hand, there exists a strong repulsive force between atoms on the same site, caused by the overlapping of their electron clouds. The interaction is then to a high degree truly on-site, and it is a good approximation to set $U = 0$ for cases other than $i = j = k = l$.

We make one further radical simplification, and assume that the particles will only occupy the lowest band in the system. Again this assumption is much less serious in an optical lattice than in a real one. By adjusting the depth of the potential wells one can adjust the energy gap between the first and second band states, and make it sufficiently large compared to the atom cloud temperature that no significant amount of excitations will occur. Note that this assumption is not integral to the Hubbard model, which can equally well be used for calculations with multiple band systems.

Finally we assume that the atoms in our optical lattice system are either spinless or spin-polarized, so that the different spin states can be ignored.

After these simplifications the Hamiltonian (2.17) takes the form

$$\hat{H} = \sum_{\langle i,j \rangle} t_{ij} \hat{a}_i^\dagger \hat{a}_j + \frac{U}{2} \sum_i \hat{a}_i^\dagger \hat{a}_i^\dagger \hat{a}_i \hat{a}_i \tag{2.21}$$

where $\langle ... \rangle$ denotes a summation over neighboring sites. Writing the potential term of the above Hamiltonian in terms of the number operator $n_i = a_i^\dagger a_i$, we get

$$V_P^{bos} = \frac{U}{2} \sum_i \hat{a}_i^\dagger \hat{a}_i^\dagger \hat{a}_i \hat{a}_i = \frac{U}{2} \sum_i \hat{a}_i^\dagger (\hat{a}_i \hat{a}_i^\dagger - 1) \hat{a}_i = \frac{U}{2} \sum_i (n_i^2 - n_i)$$

for bosons, and

$$V_P^{fer} = \frac{U}{2}\sum_i \hat{a}_i^\dagger \hat{a}_i^\dagger \hat{a}_i \hat{a}_i = \frac{U}{2}\sum_i \hat{a}_i^\dagger (1 - \hat{a}_i \hat{a}_i^\dagger)\hat{a}_i = \frac{U}{2}\sum_i (n_i - n_i^2)$$

for fermions. These expressions can be further simplified by writing

$$\sum_i \hat{n}_i^2 = \sum_i (\hat{n}_i(\hat{n}_i - 1) + \hat{n}_i), \tag{2.22}$$

after which we have

$$V_P^{bos} = \frac{U}{2}\sum_i \hat{n}_i(\hat{n}_i - 1), \qquad V_P^{fer} = -\frac{U}{2}\sum_i \hat{n}_i(\hat{n}_i - 1) = -V_P^{bos}$$

These potential terms give U energy for each separate pair of particles in a site. That is, the particles do not interact with themselves (Each pair is counted twice, which is countered by the factor $\frac{1}{2}$).

Note that in the case of spin-polarized fermions, of which there can never be more than one in a lattice site, the potential term of the Hamiltonian becomes identically zero. The Hubbard model in this case reduces to a simple non-interacting tight-binding model. We can therefore write the Hamiltonian for both bosons and fermions in the form

$$\hat{H} = \sum_{\langle i,j \rangle} t_{ij} \hat{a}_i^\dagger \hat{a}_j + \frac{U}{2}\sum_i \hat{n}_i(\hat{n}_i - 1). \tag{2.23}$$

An external potential can be added to the system by introducing to the Hamiltonian (2.23) an additional term

$$V_{ext} = \sum_i V_i \hat{n}_i, \tag{2.24}$$

where V_i is the potential on the lattice site i.

Matrix Form of the Hamiltonian

The states of a multi-particle system in a lattice can be handily expressed in the Fock-space in the so-called occupation number representation, where we choose some single-particle basis, and then express the multi-particle state in terms of integer occupation numbers corresponding to each basis state. In our case the logical choice of basis is the Wannier basis, and a general multi-particle state is written as

$$\psi = |n_1\, n_2\, n_3\, \cdots\rangle, \tag{2.25}$$

where n_i is the occupation of the Wannier state $\phi_i(\mathbf{x})$, or the number of particles in the lattice site i. These states are all mutually orthogonal, and we take them to be normalized to unity, i.e.

$$\langle \psi_i | \psi_j \rangle = \delta_{ij}.$$

With the Fock-states one can easily form a basis for the multi-particle system by taking all the possible ways to place the particles into the sites. For a spin-less fermionic system, where one can only have either zero or one particles in a lattice site, the number of these states is

$$N_{states} = \frac{N_s!}{N_p!(N_s - N_p)!}, \tag{2.26}$$

where N_s is the number of the lattice sites and N_p is the number of the particles. This is simply a binomial coefficient, giving the number of different ways to choose N_p sites out of N_s. The particles are indistinguishable, so the order does not matter. For bosons computing the number of the states is a bit trickier. An algorithm for it is given in section 4.1.

The elements of the Hamiltonian matrix are transition probabilities between the basis states. For example, for a two-particle system with three lattice sites, one could write

$$H = \begin{pmatrix} \langle 2\,0\,0|\hat{H}|2\,0\,0\rangle & \langle 200|\hat{H}|1\,1\,0\rangle & \cdots & \langle 2\,0\,0|\hat{H}|0\,0\,2\rangle \\ \langle 1\,1\,0|\hat{H}|2\,0\,0\rangle & & & \\ \langle 1\,0\,1|\hat{H}|2\,0\,0\rangle & & & \\ \vdots & & \ddots & \\ \langle 0\,0\,2|\hat{H}|2\,0\,0\rangle & & & \langle 0\,0\,2|\hat{H}|0\,0\,2\rangle \end{pmatrix}.$$

The dimension of the Hamiltonian matrix matches the number of basis states, and thus increases very quickly as the size of the system increases.

We derived the Hubbard model above for an infinitely large lattice. However, in order to perform numerical computations with it, we would like to describe our system using a finite sized Hamiltonian. This is achieved by choosing a suitably sized unit cell out of the lattice, and then applying periodic boundary conditions by mapping hops going out from the other side of the cell into the sites on the opposite side.

The one-particle wave functions in an infinite lattice are Bloch-waves (2.7). They can be expressed as linear combinations of Wannier functions as in (2.8)

$$\varphi_{\mathbf{k}}(\mathbf{x}) = \sum_{\mathbf{R}} e^{i\mathbf{k}\cdot\mathbf{R}} \phi(\mathbf{x} - \mathbf{R}), \tag{2.27}$$

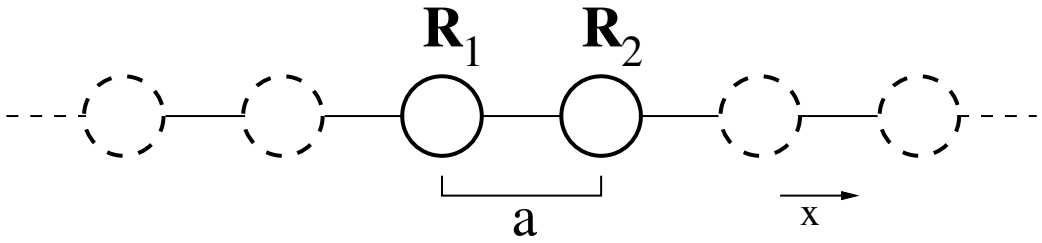

Figure 2.2: A linear chain with a two site unit cell.

if the lattice has a unit cell of one site. This generalizes as per (2.12) to

$$\varphi_{\mathbf{k}}(\mathbf{x}) = \sum_{\mathbf{R}} e^{i\mathbf{k}\cdot\mathbf{R}} \sum_{n=1}^{N_s} c_n \phi(\mathbf{x} - \mathbf{a}_n - \mathbf{R}), \tag{2.28}$$

for a unit cell containing N_s sites.

Let us compute the matrix form of the Hamiltonian for a simple linear chain with one particle per unit cell (see figure 2.2). The Hubbard Hamiltonian describing this system is

$$\hat{H} = \sum_i \left(t_{i,i+1} \hat{a}^\dagger_{i+1} \hat{a}_i + t_{i,i-1} \hat{a}^\dagger_{i-1} \hat{a}_i \right),$$

where we have left out the interaction term, because it is of no consequence in a single-particle system.

For demonstrative reasons we will choose a unit cell of two lattice sites. We will also take the hopping term to be the same for all hops, and mark $t_{ij} = -t$ for all i and j. Choosing some arbitrary two adjacent lattice sites as our point of interest, we mark their locations with R_1 and R_2. The Hamiltonian for this single unit cell is

$$\hat{H} = -t \left(\hat{a}^\dagger_{R_1+a} \hat{a}_{R_1} + \hat{a}^\dagger_{R_1-a} \hat{a}_{R_1} + \hat{a}^\dagger_{R_2+a} \hat{a}_{R_2} + \hat{a}^\dagger_{R_2-a} \hat{a}_{R_2} \right), \tag{2.29}$$

where a is the site separation.

The Hamiltonian in the above form includes creation and annihilation operators corresponding to sites other than the two in our chosen unit cell. This can be fixed by applying periodic boundary conditions by noting that from (2.28) follows a similar equation for the corresponding creation operators

$$\hat{\varphi}_k(x) = \sum_R e^{ikR} \left(c_1 \hat{a}^\dagger_R + c_2 \hat{a}^\dagger_{R+a} \right). \tag{2.30}$$

Because the lattice is infinite, we can substitute $R = R + 2a$ into (2.30) without changing anything. This gives

$$\begin{aligned}\hat{\varphi}_k(x) &= \sum_R e^{ik(R+2a)} \left(c_1 \hat{a}^\dagger_{R+2a} + c_2 \hat{a}^\dagger_{R+3a} \right) \\ &= \sum_R e^{ikR} \left(c_1 e^{2ika} \hat{a}^\dagger_{R+2a} + c_2 e^{2ika} \hat{a}^\dagger_{R+3a} \right). \end{aligned} \tag{2.31}$$

Comparing (2.31) with (2.30) we get

$$\hat{a}^\dagger_{R+2a} = e^{-2ika} \hat{a}^\dagger_R, \qquad \hat{a}^\dagger_{R+a} = e^{2ika} \hat{a}^\dagger_{R+3a},$$

where R is any Bravais lattice vector. Substituting $R = R_1$ into the first expression, and $R = R_1 - 2a$ to the second one gives

$$\hat{a}^\dagger_{R_1+2a} = e^{-2ika} \hat{a}^\dagger_{R_1}, \qquad \hat{a}^\dagger_{R_1-a} = e^{2ika} \hat{a}^\dagger_{R_1+a}. \tag{2.32}$$

Using equations (2.32) we can shift the hopping terms in (2.29) so that they all operate on sites within the chosen unit cell. Noting that $R_2 + a = R_1 + 2a$, this gives

$$\begin{aligned}\hat{H} &= -t \left(\hat{a}^\dagger_{R_1+a} \hat{a}_{R_1} + e^{2ika} \hat{a}^\dagger_{R_1+a} \hat{a}_{R_1} + e^{-2ika} \hat{a}^\dagger_{R_1} \hat{a}_{R_2} + \hat{a}^\dagger_{R_2-a} \hat{a}_{R_2} \right) \\ &= -t \left((1 + e^{2ika}) \hat{a}^\dagger_{R_2} \hat{a}_{R_1} + (1 + e^{-2ika}) \hat{a}^\dagger_{R_1} \hat{a}_{R_2} \right). \end{aligned}$$

Similarly for any lattice configuration, one can handle hops out of the unit cell by shifting the destination by a Bravais vector, and introducing the phase term corresponding to the Bloch wave vector.

The Hamiltonian matrix for the linear chain with a two-site unit-cell is then

$$H = \begin{pmatrix} \langle 10|\hat{H}|10\rangle & \langle 10|\hat{H}|01\rangle \\ \langle 01|\hat{H}|10\rangle & \langle 01|\hat{H}|01\rangle \end{pmatrix} \tag{2.33}$$

$$= -t \begin{pmatrix} 0 & 1 + e^{-2ika} \\ 1 + e^{2ika} & 0 \end{pmatrix}. \tag{2.34}$$

A possible external potential of the form of (2.24) would manifest itself as diagonal terms in the Hamiltonian, giving

$$H = \begin{pmatrix} V_1 & -t(1 + e^{-2ika}) \\ -t(1 + e^{2ika}) & V_2 \end{pmatrix}. \tag{2.35}$$

We can only set the potential independently in as many sites as are contained in the chosen unit cell. Modeling a system with a parabolic confinement

potential therefore requires a relatively large unit cell, and consequently a large Hamiltonian.

It is relatively straightforward to form the Hubbard Hamiltonian for any single-particle system, without having to perform any calculations. Every element of the Hamiltonian corresponds to a hop from a lattice site to another. One only needs to set each element to the value of the hopping parameter corresponding to that hop, taking a sum if there are multiple ways the hop can occur, multiply by a phase factor for hops between unit cells, and set the diagonal elements to the value of the potential on the corresponding site.

2.2.2 Band Structure

In the context of the tight-binding approximation, the formation of energy bands is most easily understood by starting from the limit of no overlap between the wave functions. The atoms are then confined each to their own lattice site, and are on one of the discrete energy states of the potential well. When the depth of the potential wells is slowly decreased, and the wave functions start to mingle allowing tunneling to occur from one site to the next, the localized states turn into Bloch-wave type states that stretch across the whole lattice.

In the limit of small overlap, these Bloch-waves can be thought of as linear combinations of the localized states in the form of (2.12)

$$\varphi_{\alpha\mathbf{k}}(\mathbf{r}) = \sum_{\mathbf{R}} e^{i\mathbf{k}\cdot\mathbf{R}} \sum_{n=1}^{N_s} c_{n\alpha}\psi_\alpha(\mathbf{r} - \mathbf{R}_i - \mathbf{a}_n), \tag{2.36}$$

where $\mathbf{R}$ is a Bravais lattice vector, n denotes a lattice site in the unit cell, $\psi_\alpha(\mathbf{x} - \mathbf{R}_i - \mathbf{a}_n)$ is the localized wave function corresponding to the energy eigenstate α and centered on the lattice site marked by the Bravais lattice vector $\mathbf{R}_i$ and the basis vector $\mathbf{a}_n$.

For any $\mathbf{k}$, the number of different energies, or the number of energy bands, is equal to the number of single-particle states in the unit cell. Because there is an infinite number of energy eigenstates for each of the potential wells, there is in general an infinite number of bands. In this work I make the assumption, that only the lowest energy eigenstate in each well will be used. The number of energy bands will therefore be determined simply by the number of sites in the unit cell.

The energy of a Bloch-wave of the form (2.36) is based on the energy of the localized state it derives from. It is shifted slightly by the lowering of the potential, and when the wave functions start to overlap, it acquires a component dependent on the phase differences between amplitudes in the lattice

sites. The phase differences modify the shape of the resulting probability distribution by introducing varying amounts of either constructive or destructive interference in the area of overlap between the lattice sites. Correspondingly the particles are either dispersed more readily to the area between the sites, or become concentrated nearer to the bottoms of the wells. The more concentrated states have higher total energy, whereas the more spread-out ones have lower energy.

In (2.36), the amplitudes in the sites of the unit cell are given by the factors c_n. These are obtained by solving the eigenvectors of the Hamiltonian of the system. Each of the N_s eigenvectors is associated with an eigenenergy, which depends on the phase differences between sites of the unit cell, determined by c_n, and furthermore on the phase difference between adjacent unit cells, determined by the phase term $e^{i\mathbf{k}\cdot\mathbf{R}}$ of the Bloch-wave. The result is then N_s different energies, each of which is in general a function of the Bloch wave vector $\mathbf{k}$. These are the energy bands.

Flat-Band

A flat-band is a band whose energy is independent of the wave vector, at least approximately and for a certain $\mathbf{k}$-interval. Because the group velocity of a particle on the band n is given by [11, p. 192]

$$v_g = \frac{1}{\hbar}\nabla_{\mathbf{k}} E_n(\mathbf{k}), \tag{2.37}$$

it follows that for a particle on a flat-band, the velocity goes to zero. This is equivalent to the particle having an infinite effective mass [11, p. 191]. This property leads to the phenomenon, that particles occupying a flat-band state will not move, but remain stationary within the lattice.

Some heuristic arguments will now be given for determining conditions in which a flat-band occurs in the context of the tight-binding model. For a more rigorous treatment see for example [20].

It was argued above that the $\mathbf{k}$-dependency in the energy bands is the result of interference caused by phase differences between the wave functions of neighboring unit cells. It is therefore straightforward to come up with one situation in which a flat-band emerges. Specifically, when the amplitudes in the unit cell come up in such a way, that on the unit cell borders one of the adjacent sites always has a zero amplitude. In such a case the value of $\mathbf{k}$ clearly makes no difference, as the parts of the wave function in different unit cells will be totally separated from each other with no overlap.

The next question then is: what kind of lattices support an energy eigenstate that has a zero amplitude on at least one of the unit cell sites. In order

to answer this question it is helpful to thing how the Hamiltonian through Schrödinger equation determines the time evolution of a state.

Each element in the Hamiltonian corresponds to a transition amplitude from one site to another. Lets take a very simple system of two lattice sites and one particle, and describe the connection between the sites with a hopping term t_h. The tight-binding Hamiltonian describing this system is

$$H = \begin{pmatrix} 0 & t_h^* \\ t_h & 0 \end{pmatrix}.$$

Let us then set the system into an initial state where all of the amplitude is located in one of the sites. This state is then depicted by a state vector $\psi(0) = c|10\rangle = |c\,0\rangle$ (Using the occupation number representation in the Wannier basis). After a differentially small time of δt, the system is in the configuration

$$\psi(\delta t) = \psi(0) + \frac{d\psi}{dt}\delta t = \psi(0) - \frac{i}{\hbar}\hat{H}\psi\delta t,$$

and using the matrix notation

$$\psi(\delta t) - \psi(0) = -\frac{i}{\hbar}\hat{H}\psi\delta t = -\frac{i}{\hbar}\begin{pmatrix} 0 & t_h \\ t_h & 0 \end{pmatrix}\begin{pmatrix} c \\ 0 \end{pmatrix}\delta t = \begin{pmatrix} 0 \\ -ict_h\delta t/\hbar \end{pmatrix}.$$

The result

$$\psi(\delta t) = \begin{pmatrix} c \\ -ict_h\delta t/\hbar \end{pmatrix},$$

shows that the amplitude on site 1 has flowed to site 2, and that the flow rate is proportional to the hopping term t_h, as well as the amplitude c in the source site.

It is seen that the time-evolution of a single-particle state in the tight-binding model is essentially very simple, and consists only of amplitude flowing between the lattice sites in proportion with the associated hopping terms. If there was a lattice site with no amplitude in it, there would necessarily be a flow of amplitude to it from the neighboring sites. The only way to make the situation stationary then, would be to choose the amplitudes on its neighboring lattices so, that the flows would perfectly cancel out each other. In section 3 I will give some examples of lattices in which this happens.

2.2.3 Current in a Hubbard Ring

I wish to study the current flowing in a circular one-dimensional ring formed from a Hubbard chain, when it is placed in a homogeneous magnetic field passing perpendicularly through it. To achieve this I will first consider the

effect of a magnetic field on the Hamiltonian of a lattice system, and its energy eigenstates, in a general case. I then move to the case of the Hubbard ring, and use the modified Hamiltonian to derive a current operator, whose expectation values give the amount of current flow for a certain state and a given magnetic field. Throughout this section I will use a unit system in which $\hbar = 1$, and I will denote the charge of the particles by e.

The prospect of using a magnetic field to induce a current is of course not applicable to an optical lattice system containing neutral atoms. Although there are ways to build ring shaped optical lattices, and even to induce and study currents in them (see [21]), I will not here go into that. My aim is only to study the properties of the lattice structures, especially the effect of the flat-bands on their conductive properties. For this purpose it is sufficient to use the familiar language of charged particles in a magnetic field, and the results will be applicable to the corresponding linear optical chains.

The Single-Particle Hamiltonian and Its Eigenstates

Our task is to find out how the single-particle Hamiltonian (2.14) is modified by the presence of an external magnetic field, and how this will affect the form of its eigenfunctions (2.7). We start by introducing the electromagnetic potential terms into the single particle Lagrangian, which results in

$$\begin{aligned}\tilde{\mathcal{L}}(\mathbf{x}, \dot{\mathbf{x}}) &= \frac{1}{2}m\dot{\mathbf{x}}^2 + V_L(\mathbf{x}) - e\mathbf{A}\dot{\mathbf{x}} - eV_E(\mathbf{x}) \\ &= \mathcal{L}(\mathbf{x}, \dot{\mathbf{x}}) - e\mathbf{A}\dot{\mathbf{x}},\end{aligned}$$

where $\mathcal{L}$ is the Lagrangian for a particle with no external field, $\mathbf{A}$ is a vector potential corresponding to some arbitrary magnetic field, and V_E is the electric scalar potential. We take there to be no external electric field, and thus can choose a gauge in which $V_E(\mathbf{x}) = 0$. The single particle Hamiltonian is then obtained from the Lagrangian through a Legendre transformation

$$\begin{aligned}\tilde{\hat{h}}(\mathbf{x}, \mathbf{p}) &= \dot{\mathbf{x}}\mathbf{p} - \tilde{\mathcal{L}} \\ &= \dot{\mathbf{x}}\mathbf{p} - \mathcal{L} + e\mathbf{A}\dot{\mathbf{x}} \\ &= \dot{\mathbf{x}}(\mathbf{p} + e\mathbf{A}) - \mathcal{L} \\ &= \hat{h}(\mathbf{x}, \mathbf{p} + e\mathbf{A}).\end{aligned}$$

The effect of the magnetic field is thus taken into account simply by substituting

$$\mathbf{p} = \mathbf{p} + e\mathbf{A}$$

into the single-particle Hamiltonian. By this substitution the Hamiltonian (2.14) becomes

$$\tilde{\hat{h}} = \frac{1}{2m}\left(\hat{\mathbf{p}} + e\mathbf{A}\right)^2 + V(\mathbf{x}).$$

The energy eigenstates of this Hamiltonian are of the form

$$\tilde{\varphi}_{\mathbf{k}}(\mathbf{x}) = e^{-ie\lambda}\varphi_{\mathbf{k}}(\mathbf{x}), \tag{2.38}$$

where $\varphi_{\mathbf{k}}(\mathbf{x})$ (see 2.7) is a Bloch-wave state of the system without the magnetic field and

$$\lambda(\mathbf{x}) = \int_{\mathbf{x}_0}^{\mathbf{x}} d\mathbf{y}\mathbf{A}(\mathbf{y}), \tag{2.39}$$

where x_0 is an arbitrary point. To prove this we first use the fact that

$$\partial_{\mathbf{x}}\lambda(\mathbf{x}) = \partial_{\mathbf{x}}\int_{\mathbf{x}_0}^{\mathbf{x}} d\mathbf{y}\mathbf{A}(\mathbf{y}) = \mathbf{A}(\mathbf{x}),$$

to show that for an arbitrary function $f(\mathbf{x})$

$$\begin{aligned}
&e^{-ie\lambda}\hat{\mathbf{p}}^2 e^{ie\lambda} f(\mathbf{x}) \\
=&e^{-ie\lambda}\hat{\mathbf{p}}\left[e(\partial_{\mathbf{x}}\lambda)e^{ie\lambda} + e^{ie\lambda}\hat{\mathbf{p}}\right] f(\mathbf{x}) \\
=&e^{-ie\lambda}\left[e(\hat{\mathbf{p}}\partial_{\mathbf{x}}\lambda)e^{ie\lambda} + e^2(\partial_{\mathbf{x}}\lambda)^2 e^{ie\lambda} + 2e(\partial_{\mathbf{x}}\lambda)e^{ie\lambda}\hat{\mathbf{p}} + e^{ie\lambda}\hat{\mathbf{p}}^2\right] f(\mathbf{x}) \\
=&\left[e^2\mathbf{A}^2 + e(\hat{\mathbf{p}}\mathbf{A}) + 2e\mathbf{A}\hat{\mathbf{p}} + \hat{\mathbf{p}}^2\right] f(\mathbf{x}) \\
=&\left[e^2\mathbf{A}^2 + e\hat{\mathbf{p}}\mathbf{A} + e\mathbf{A}\hat{\mathbf{p}} + \hat{\mathbf{p}}^2\right] f(\mathbf{x}) = (\hat{\mathbf{p}} + e\mathbf{A})^2 f(\mathbf{x}),
\end{aligned} \tag{2.40}$$

where in the second to last equality we have used the chain rule in the form

$$\hat{\mathbf{p}}\mathbf{A}f(\mathbf{x}) = (\hat{\mathbf{p}}\mathbf{A})f(\mathbf{x}) + \mathbf{A}\hat{\mathbf{p}}f(\mathbf{x}).$$

Using (2.40) it is then easy to show that

$$\begin{aligned}
\tilde{\hat{h}}\tilde{\varphi}(\mathbf{x}) &= \left[\frac{1}{2m}\left(\hat{\mathbf{p}} + e\mathbf{A}\right)^2 + V(\mathbf{x})\right]\tilde{\varphi}_{\mathbf{k}}(\mathbf{x}) \\
&= \left[\frac{1}{2m}e^{-ie\lambda}\hat{\mathbf{p}}^2 e^{ie\lambda} + V(\mathbf{x})\right] e^{-ie\lambda}\varphi_{\mathbf{k}}(\mathbf{x}) \\
&= e^{-ie\lambda}\left[\frac{\hat{\mathbf{p}}^2}{2m} + V(\mathbf{x})\right]\varphi_{\mathbf{k}}(\mathbf{x}) \\
&= e^{-ie\lambda}E_{\mathbf{k}}\varphi_{\mathbf{k}}(\mathbf{x}) = E_{\mathbf{k}}\tilde{\varphi}_{\mathbf{k}}(\mathbf{x}),
\end{aligned}$$

which proves that (2.38) is indeed an eigenstate of $\tilde{\hat{h}}$.

The Hubbard Hamiltonian

Deriving the multi-particle Hubbard Hamiltonian (2.23) in the case of an external magnetic field is now straightforward. The only modification to it comes through the hopping matrix (2.18), which after substituting (2.2.3) takes the form

$$\tilde{t}_{ij} = \int dx^3 \phi^*(\mathbf{x} - \mathbf{R}_i) \left[\frac{1}{2m} \left(\hat{\mathbf{p}} + e\mathbf{A} \right)^2 + V(\mathbf{x}) \right] \phi(\mathbf{x} - \mathbf{R}_j). \tag{2.41}$$

Using (2.40) we write (2.41) as

$$\tilde{t}_{ij} = \int dx^3 \phi^*(\mathbf{x} - \mathbf{R}_i) e^{-ie\lambda} \left[\frac{1}{2m} \hat{\mathbf{p}}^2 + V(\mathbf{x}) \right] e^{ie\lambda} \phi(\mathbf{x} - \mathbf{R}_j). \tag{2.42}$$

Now by defining

$$\tilde{\phi}(\mathbf{x} - \mathbf{R}_i) = e^{ie\lambda(\mathbf{x})} \phi(\mathbf{x} - \mathbf{R}_i),$$

we can rewrite (2.42) as

$$\tilde{t}_{ij} = \int dx^3 \tilde{\phi}^*(\mathbf{x} - \mathbf{R}_i) \left[\frac{\hat{\mathbf{p}}}{2m} + V(\mathbf{x}) \right] \tilde{\phi}(\mathbf{x} - \mathbf{R}_j),$$

where similarly to (2.38), the effect of the external field is revealed to be only a modification of the phases of the Wannier functions.

Now if the Wannier functions are strongly localized, and on the other hand, the vector potential $\mathbf{A}$ varies slowly in the scale of the lattice parameters, we can make the approximation

$$\tilde{\phi}(\mathbf{x} - \mathbf{R}_i) = e^{ie\lambda(\mathbf{R}_i)} \phi(\mathbf{x} - \mathbf{R}_i).$$

The modified hopping matrix then becomes

$$\begin{aligned} \tilde{t}_{ij} &= e^{ie(\lambda(\mathbf{R}_j) - \lambda(\mathbf{R}_i))} \int dx^3 \phi^*(\mathbf{x} - \mathbf{R}_i) \left[\frac{\hat{\mathbf{p}}}{2m} + V(\mathbf{x}) \right] \phi(\mathbf{x} - \mathbf{R}_j) \\ &= t_{ij} e^{ie(\lambda(\mathbf{R}_j) - \lambda(\mathbf{R}_i))}, \end{aligned}$$

and the Hamiltonian (2.23) transforms to

$$\tilde{\hat{H}} = \sum_{\langle i,j \rangle} t_{ij} e^{ie(\lambda(\mathbf{R}_j) - \lambda(\mathbf{R}_i))} \hat{a}_i^\dagger \hat{a}_j + \frac{U}{2} \sum_i \hat{n}_i (\hat{n}_i - 1), \tag{2.43}$$

where

$$\begin{aligned} \lambda(\mathbf{R}_j) - \lambda(\mathbf{R}_i) &= \int_{\mathbf{x}_0}^{\mathbf{R}_j} d\mathbf{y} \mathbf{A}(\mathbf{y}) - \int_{\mathbf{x}_0}^{\mathbf{R}_i} d\mathbf{y} \mathbf{A}(\mathbf{y}) \\ &= \int_{\mathbf{R}_i}^{\mathbf{R}_j} d\mathbf{y} \mathbf{A}(\mathbf{y}). \end{aligned} \tag{2.44}$$

The Current Operator for a Ring

We will take our ring to lie on the xy-plane, and the external magnetic field direction to be along the z-axis. The homogeneous magnetic field and the corresponding vector potential along the ring, expressed in cylindrical coordinates, are then

$$\mathbf{B} = B\hat{z}, \qquad \mathbf{A} = A_\theta\hat{\theta}, \qquad A_\theta = B\frac{R}{2} = \frac{\Phi}{2\pi R}, \tag{2.45}$$

where R is the radius of the ring and $\Phi = \pi R^2 B$ is the magnetic flux through it. We denote the azimuth angle by θ.

In the cylindrical coordinate system, the only coordinate needed for describing the ring system is the angle θ. The Hamiltonian (2.2.3) can be written in the form

$$\tilde{\hat{h}} = \frac{1}{2m}\left(\hat{p} + eA_\theta\right)^2 + V(\theta) = \frac{1}{2m}\left(-\frac{i\hbar}{R}\frac{\partial}{\partial\theta} + \frac{e\Phi}{2\pi R}\right)^2 + V(\theta),$$

and the Bloch waves (2.7) in the form

$$\varphi_m(\theta) = e^{im\theta}u_m(\theta),$$

where $m\hbar = Rk\hbar$ is the angular momentum. There is now a restriction on the values of the angular wave number m, due to the fact that the ends of the chain are connected and therefore the values of the wave function need to match for $\theta = 0$ and $\theta = 2\pi$. m thus has to fulfill

$$u_m(0) = e^{i2\pi m}u_m(2\pi) \Rightarrow e^{i2\pi m} = 1 \Rightarrow m \in \mathbb{Z}, \tag{2.46}$$

where we have used the fact that $u_m(0) = u_m(2\pi)$, which follows from u_m's periodicity. The energy spectrum of the ring therefore becomes discrete, consisting of those energies E_m for which m satisfies the boundary condition.

If we assume that one hop on the chain is very short compared to the length of the whole ring, we can, in the expression (2.39) for λ, perform the integration along the perimeter of the ring, and it simplifies to

$$\lambda(\theta) = \int_{\theta_0}^{\theta} Rd\theta\,\mathbf{A} = \frac{\Phi}{2\pi R}\int_{\theta_0}^{\theta} Rd\theta\,\hat{\theta} = \frac{\Phi}{2\pi}(\theta - \theta_0), \tag{2.47}$$

which allows us to write the eigenstates (2.38) of $\tilde{\hat{h}}$ in the form

$$\tilde{\varphi}_m(\theta) = e^{-\frac{ie\Phi}{2\pi}\theta}\varphi_m(\theta) = e^{i(m-\frac{e\Phi}{2\pi})\theta}u_m(\theta), \tag{2.48}$$

where we have chosen $\theta_0 = 0$. Similarly to (2.46), it follows from (2.48) that

$$m - \frac{e\Phi}{2\pi} \doteq m - \Phi' \in \mathbb{Z}. \tag{2.49}$$

Changing the magnetic field therefore changes the boundary condition. Consequently the energy spectrum shifts to consist of the energies E_m for which this new condition is fulfilled, and the energies thus become dependent on the flux Φ. I will mark these energies by $\tilde{E}_m$. Notice that if $\Phi' \in \mathbb{Z}$ the energy spectrum of the ring will exactly match that of the zero flux case, but the energies will correspond to different values of the angular momentum.

It turns out that the current operator can be derived in a simple manner from the Hamiltonian of the system. Starting from the eigenvalue equation

$$\tilde{\hat{h}}\tilde{\varphi} = \tilde{E}_m\tilde{\varphi}, \tag{2.50}$$

and multiplying it from the left by $\int_0^{2\pi} Rd\varphi\, \tilde{\varphi}^*$ we get

$$\int_0^{2\pi} Rd\theta\, \tilde{\varphi}^*\tilde{\hat{h}}\tilde{\varphi} = \tilde{E}_m \int_0^{2\pi} Rd\theta\, \tilde{\varphi}^*\tilde{\varphi} = \tilde{E}_m. \tag{2.51}$$

Taking now a derivate of (2.51) with respect to the magnetic flux leads to

$$\begin{aligned}
\frac{d\tilde{E}_m}{d\Phi} &= \int_0^{2\pi} Rd\theta\, \left[\frac{d\tilde{\varphi}^*}{d\Phi}\tilde{\hat{h}}\tilde{\varphi} + \tilde{\varphi}^*\frac{d\tilde{\hat{h}}}{d\Phi}\tilde{\varphi} + \tilde{\varphi}^*\tilde{\hat{h}}\frac{d\tilde{\varphi}}{d\Phi}\right] \\
&= \int_0^{2\pi} Rd\theta\, \left[ie\frac{d\lambda}{d\Phi}\tilde{\varphi}^*\tilde{\hat{h}}\tilde{\varphi} + \tilde{\varphi}^*\frac{d\tilde{\hat{h}}}{d\Phi}\tilde{\varphi} - ie\frac{d\lambda}{d\Phi}\tilde{\varphi}^*\tilde{\hat{h}}\tilde{\varphi}\right] \\
&= \int_0^{2\pi} Rd\theta\, \tilde{\varphi}^*\frac{d}{d\Phi}\left(\frac{1}{2m}\left(\hat{p} + \frac{e\Phi}{2\pi R}\right)^2 + V(\mathbf{x})\right)\tilde{\varphi} \\
&= \frac{1}{m}\frac{e}{2\pi}\int_0^{2\pi} d\theta\, \tilde{\varphi}^*\left(\hat{p} + \frac{e\Phi}{2\pi R}\right)\tilde{\varphi}.
\end{aligned} \tag{2.52}$$

We denote the modified crystal momentum by $\tilde{\hat{p}} = \hat{p} + \frac{e\Phi}{2\pi R}$. Taking then the real part of (2.52) gives

$$\begin{aligned}
Re\left(\frac{d\tilde{E}_m}{d\Phi}\right) = \frac{d\tilde{E}_m}{d\Phi} &= \frac{1}{m}\frac{e}{2\pi}\int_0^{2\pi} d\theta\, Re(\tilde{\varphi}^*\tilde{\hat{p}}\tilde{\varphi}) \\
&= \frac{e}{2\pi}\int_0^{2\pi} d\theta\, \frac{1}{2m}(\tilde{\varphi}^*\tilde{\hat{p}}\tilde{\varphi} - \tilde{\varphi}\tilde{\hat{p}}^*\tilde{\varphi}^*).
\end{aligned}$$

The term inside the integral in the above equation is just the definition of the probability current j [18, p. 56]. We can therefore write

$$\frac{d\tilde{E}_m}{d\Phi} = \frac{e}{2\pi}\int_0^{2\pi} d\theta\, j = ej = c, \tag{2.53}$$

where c is the charge current, and we have used the fact that j must be independent of θ.

Taking the flux derivative of the equation (2.50) now leads to

$$\begin{aligned}
&\frac{\partial\tilde{\hat{h}}}{\partial\Phi}\tilde{\varphi} + \tilde{\hat{h}}\frac{\partial\tilde{\varphi}}{\partial\Phi} = \frac{\partial\tilde{E}_m}{\partial\Phi}\tilde{\varphi} + \tilde{E}_m\frac{\partial\tilde{\varphi}}{\partial\Phi} \\
\Rightarrow &\frac{\partial\tilde{\hat{h}}}{\partial\Phi}\tilde{\varphi} - \frac{ie\theta}{2\pi}\tilde{\hat{h}}\tilde{\varphi} = \frac{\partial\tilde{E}_m}{\partial\Phi}\tilde{\varphi} - \frac{ie\theta}{2\pi}\tilde{E}_m\tilde{\varphi} \\
\Rightarrow &\frac{\partial\tilde{\hat{h}}}{\partial\Phi}\tilde{\varphi} = \frac{\partial\tilde{E}_m}{\partial\Phi}\tilde{\varphi} = c\tilde{\varphi} \;\Rightarrow\; \frac{\partial\tilde{\hat{h}}}{\partial\Phi} = \hat{c},
\end{aligned}$$

where we have first used (2.48) and then (2.50). The current operator for the single-particle case is therefore obtained simply by taking a derivative of the Hamiltonian with respect to the magnetic flux.

This same method works also in the case of an interacting multi-particle system. Taking the derivative of the Hamiltonian (2.13) (with $\hat{h}$ replaced by $\tilde{\hat{h}}$) gives

$$\begin{aligned}
\frac{\partial\hat{H}}{\partial\Phi} &= \frac{\partial}{\partial\Phi}\left(\sum_{i=1}^{N}\tilde{\hat{h}} + \sum_{1\le i<j\le N} V_I\right) \\
&= \sum_{i=1}^{N}\frac{\partial\tilde{\hat{h}}}{\partial\Phi} = \sum_{i=1}^{N}\hat{c} = \hat{C},
\end{aligned} \tag{2.54}$$

which is just the sum of the currents contributed by each of the particles.

To obtain the second quantized version of $\hat{C}$ one then needs only to take a derivative of (2.43) with respect to the magnetic flux. In the case of our one-dimensional ring this Hamiltonian takes the form

$$\tilde{\hat{H}} = \sum_{\langle i,j\rangle} t_{ij}e^{ie(\lambda(\theta_j)-\lambda(\theta_i))}\hat{a}_i^\dagger\hat{a}_j + \frac{U}{2}\sum_i \hat{n}_i(\hat{n}_i - 1).$$

By using (2.47) we get

$$\lambda(\theta_j) - \lambda(\theta_i) = \frac{\Phi}{2\pi}(\theta_j - \theta_0) - \frac{\Phi}{2\pi}(\theta_i - \theta_0) = \frac{\Phi}{2\pi}(\theta_j - \theta_i) = \Phi l_{ij},$$

where $l_{ij} = (\theta_j - \theta_i)/2\pi$ is the ratio of the i-j hop length to the length of the loop. The resulting current operator is then

$$\hat{C} = \frac{\partial \tilde{\hat{H}}}{\partial \Phi} = ie \sum_{\langle i,j \rangle} t_{ij} l_{ij} e^{ie\Phi l_{ij}} \hat{a}_i^\dagger \hat{a}_j. \tag{2.55}$$

Chapter 3

Examples of Lattices and Their Band Structures

In this chapter I present three examples of one-dimensional lattices containing a flat-band. Accompanying are plots of the band structures and some discussion about the specific properties of each lattice giving rise to that structure.

3.1 The Rake Chain

Figure 3.1 depicts a type of one dimensional lattice I call the rake chain. It is essentially a single strip cut out of a two-dimensional line centered square lattice, which is the simplest two-dimensional example of a flat-band lattice (studied for example in [22]). All of the hopping parameters have the same value of t. The Hamiltonian for this lattice, when using the primitive cell as a unit cell, is

$$\hat{H} = -t\left(\hat{a}^\dagger_{R_1+a}\hat{a}_{R_1} + \hat{a}^\dagger_{R_1-a}\hat{a}_{R_1} + \hat{a}^\dagger_{R_2+a}\hat{a}_{R_2} + \hat{a}^\dagger_{R_2-a}\hat{a}_{R_2} + \hat{a}^\dagger_{R_1}\hat{a}_{R_3} + \hat{a}^\dagger_{R_3}\hat{a}_{R_1}\right),$$

and after applying the periodic boundary conditions using

$$\hat{a}^\dagger_{R_2+a} = \hat{a}^\dagger_{R_1+2a} = e^{-2ika}\hat{a}^\dagger_{R_1}, \qquad \hat{a}^\dagger_{R_1-a} = e^{2ika}\hat{a}^\dagger_{R_1+a} = e^{2ika}\hat{a}^\dagger_{R_2}$$

(these can be derived similarly to (2.32)), we get

$$\hat{H} = -t\left(\hat{a}^\dagger_{R_2}\hat{a}_{R_1} + e^{2ika}\hat{a}^\dagger_{R_2}\hat{a}_{R_1} + e^{-2ika}\hat{a}^\dagger_{R_1}\hat{a}_{R_2} + \hat{a}^\dagger_{R_1}\hat{a}_{R_2} + \hat{a}^\dagger_{R_1}\hat{a}_{R_3} + \hat{a}^\dagger_{R_3}\hat{a}_{R_1}\right). \tag{3.1}$$

We denote a state of this chain by a vector $\psi = |n_1 n_2 n_3\rangle$, where n_i is the occupation of site i of the unit cell. For a system with one particle per unit

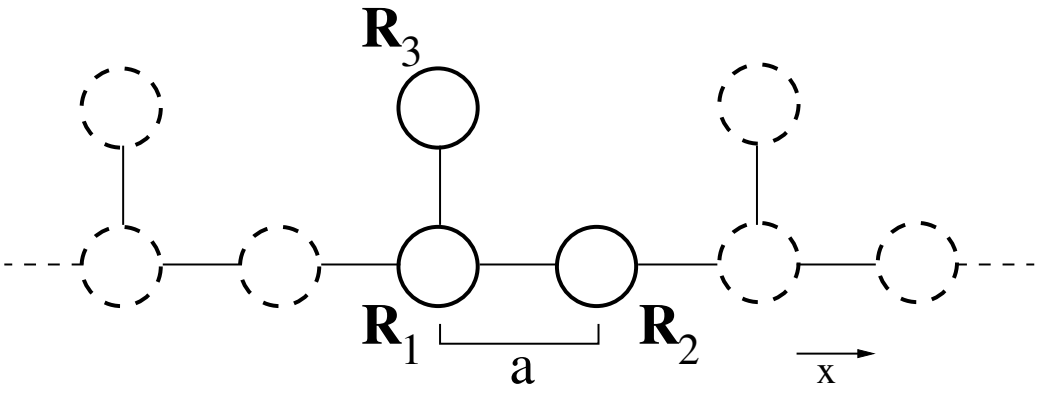

Figure 3.1: Structure of a rake chain, and the numbering used for the sites of the primitive cell.

cell, the basis consists of three states: $|100\rangle, |010\rangle, |001\rangle$. The matrix form of the Hamiltonian (3.1) is obtained as in (2.2.1)

$$\mathbf{H} = -t \begin{pmatrix} 0 & 1+e^{-2ika} & 1 \\ 1+e^{2ika} & 0 & 0 \\ 1 & 0 & 0 \end{pmatrix}. \tag{3.2}$$

From (3.2) one can compute the energy levels and the corresponding energy eigenstates of the system, by solving the eigenvalue equation

$$\mathbf{H} \begin{pmatrix} c_1 \\ c_2 \\ c_3 \end{pmatrix} = E_\alpha \begin{pmatrix} c_1 \\ c_2 \\ c_3 \end{pmatrix}.$$

We switch to a system of units in which $2a = t = 1$. The eigenenergies, seen plotted in figure 3.2, are then

$$E_1 = -\sqrt{3+2\cos k}, \qquad E_2 = 0, \qquad E_3 = \sqrt{3+2\cos k}, \tag{3.3}$$

and the energy eigenstates are

$$\psi_1 = N_1 \begin{pmatrix} E_1 \\ 1+e^{ik} \\ 1 \end{pmatrix}, \qquad \psi_2 = N_2 \begin{pmatrix} 0 \\ 1 \\ -(1+e^{-ik}) \end{pmatrix}, \qquad \psi_3 = N_3 \begin{pmatrix} E_3 \\ 1+e^{ik} \\ 1 \end{pmatrix},$$

where N_α are normalization constants.

It is easy to see how the form of the flat-band state ψ_2 comes up. In line with our earlier predictions, there is no amplitude in the corner site $\mathbf{R}_1$.

Because of this there is no overlap between wave functions in adjacent unit cells, and consequently no k-dependence in the energy. The amplitudes on sites two and three then have to come up in such a way that the total amplitude flow to site one becomes zero. If we do not care about normalization or the overall phase, we can choose the amplitude on one of these sites freely. Let us choose an amplitude of 1 for the site number two. The amplitude flow between sites is relative to the product of the hopping term and the amplitude in the source site (as was shown in the section 2.2.2). For the amplitude flow to the corner site we thus get a term $1 * 1$ from the second site of the unit cell, and a term $1 * e^{-ik}$ from the second site of the cell just left of our unit cell. Because the hopping term from the site three to the corner site is 1, the amplitude on it has to be $-(1 + e^{-ik})$, because this gives us a total flow of

$$1 * 1 + 1 * e^{-ik} - 1 * (1 + e^{-ik}) = 0,$$

and thus a stationary state.

It is possible to build more flat-band lattices by extending the rake chain by adding sites to its unit cell in a symmetrical manner (see figure 3.3). Because the amplitude in the corner site will be zero, the two n-particle strips in the unit cell will be essentially isolated from each other. Thus there will be n flat band states corresponding to the n eigenstates of an n-site linear chain. Lets mark these eigenstates by $\phi_i \, (i = 1, \ldots, n)$. The flat-band states of the infinite extended rake chain will then be of the form

$$\psi_i = N_i \begin{pmatrix} 0 \\ \phi_i \\ -(1 + e^{-ik})\phi_i \end{pmatrix}$$

(where ϕ_i is an n element column vector, and ψ_i thus a $2n+1$ element column vector).

3.2 The Sawtooth Chain

The sawtooth chain (pictured in figure 3.4) is a flat-band containing chain, that is even simpler than the rake chain in that it has a smaller primitive cell of only two sites. The flat band emerges when the hopping terms to and from the tooth tips are set to be $\sqrt{2}t$, when t is the hopping term along the baseline. The Hamiltonian, after applying the periodic boundary conditions and setting $a = t = 1$, becomes

$$\hat{H} = (e^{ik} + e^{-ik})\hat{a}^\dagger_{R_1}\hat{a}_{R_1} + \sqrt{2}(1 + e^{ik})\hat{a}^\dagger_{R_2}\hat{a}_{R_1} + \sqrt{2}(1 + e^{-ik})\hat{a}^\dagger_{R_1}\hat{a}_{R_2}. \quad (3.4)$$

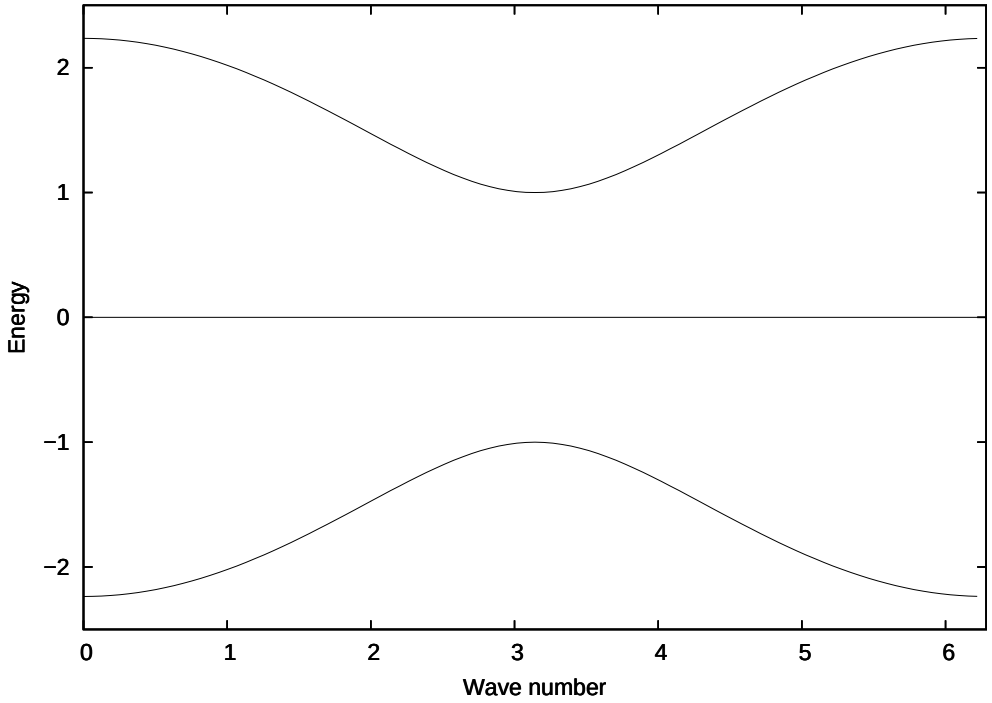

Figure 3.2: Energybands of a rake chain (see figure 3.1)

The matrix form of (3.4) is

$$\mathbf{H} = \begin{pmatrix} e^{ik} + e^{-ik} & \sqrt{2}(1 + e^{-ik}) \\ \sqrt{2}(1 + e^{ik}) & 0 \end{pmatrix}. \tag{3.5}$$

The eigenenergies for the sawtooth chain, seen plotted in figure 3.5, are

$$E_1 = -(2 + 2\cos k), \qquad E_2 = 2, \tag{3.6}$$

and the energy eigenstates are

$$\psi_1 = N_1 \begin{pmatrix} \sqrt{2}\cos\frac{k}{2} \\ e^{ik/2} \end{pmatrix}, \qquad \psi_2 = N_2 \begin{pmatrix} 1 \\ -e^{ik/2}\sqrt{2}\cos\frac{k}{2} \end{pmatrix}.$$

The effects caused by the flat-band states would be more apparent in the simulations if the flat-band was the lowest energy band. This kind of situation can be achieved by flipping the sign of the hopping term for hops along the baseline of the chain. This flips the signs of the eigenenergies (3.3) and thus changes the order of the bands, making flat band states the ground states of the system.

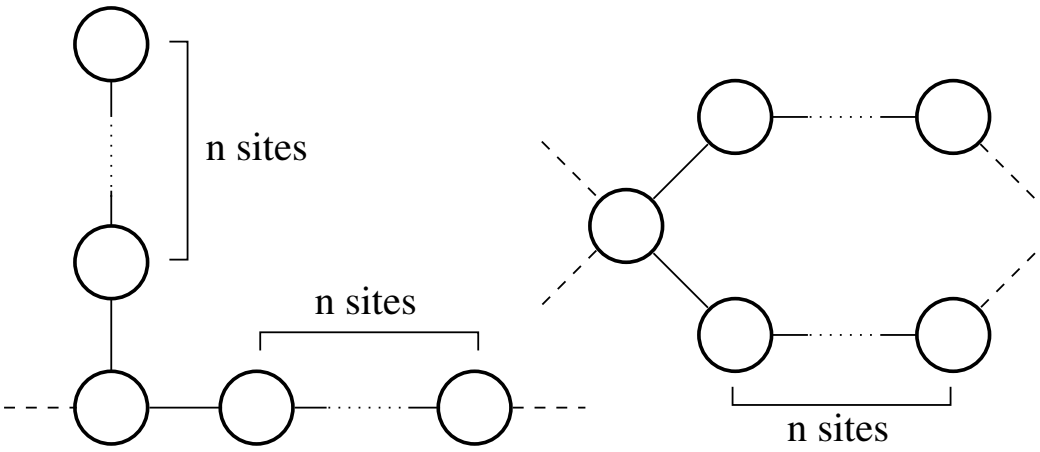

Figure 3.3: Adding sites symmetrically to the unit cells of the rake chain or the diamond chain will result in flat-band lattices containing n flat bands.

This time the flat-band state does not have a site with zero amplitude. The situation is a bit more subtle than in the rake chain. We know that the energy of a state in the Hubbard model is determined by the phase differences between neighboring sites of the lattice. Considering any single triangle of the sawtooth lattice, if the lower left corner site of it has a phase of zero, the phase of the lower right corner site will be set by the Bloch condition (2.10) to be k. Now for the flat band state ψ_2 the top site has a phase of $k/2 \pm \pi$, since $-e^{ik/2} = e^{i(k/2\pm\pi)}$. The total phase difference over a single triangle of the lattice (choosing always the angle that is smaller than π) for $0 \leq k < 2\pi$ is then

$$|k - 0| + |0 - (k/2 - \pi)| + |(k/2 + \pi) - k| = 2\pi,$$

and thus has no dependency on k. This leads to a k-independent energy, and thus a flat-band state.

It holds generally that in a Hubbard system the phases of the lowest-/highest energy eigenstate will be the ones that minimize/maximize the sum of the phase differences between neighboring sites over the lattice. This is true also of the eigenstates ψ_1 and ψ_2 of the sawtooth chain. It is a property of the triangular lattice configuration, that the maximal phase difference of 2π can always be reached by adjusting the phase in just one of the three sites. The value of k does not matter, since it only fixes the phase difference between the left and right corner sites. In cases like this a state can be flat even though it does not have a zero amplitude in any of the sites.

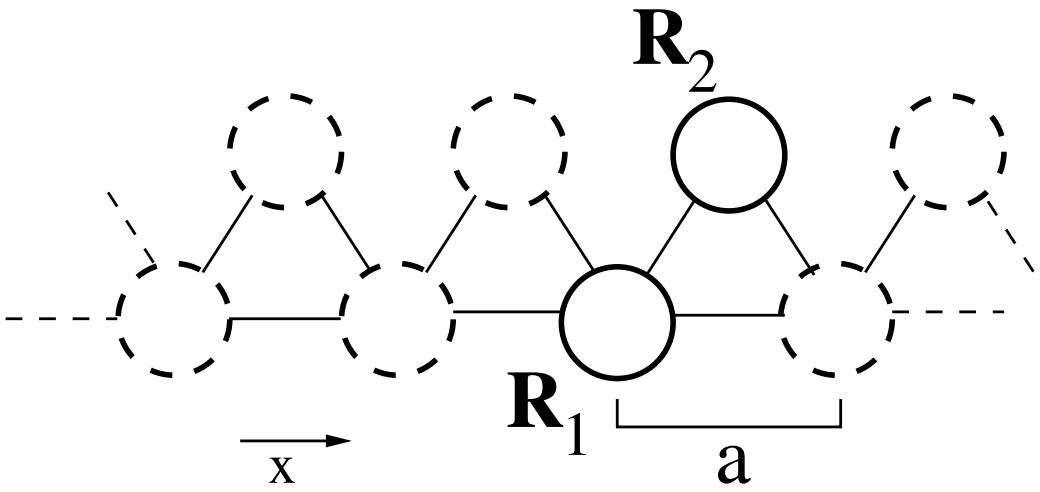

Figure 3.4: Structure of a sawtooth chain, and the numbering used for the sites of the primitive cell.

3.3 The Diamond Chain

The diamond chain is pictured in figure 3.6. It has the interesting property of containing both a flat-band and a Dirac cone at the same value of k (A Dirac cone is a conical feature in the energy band diagram, formed by the crossing of two bands with approximately linear dispersion. See figure 3.7). This creates a situation where a particle with a certain energy can have either an infinite effective mass, if it is on the flat-band, or a zero effective mass, if it is on one of the Dirac cone bands. Furthermore, the energy of the flat-band in the diamond chain can be freely adjusted by changing the hopping parameter between the sites $\mathbf{R}_2$ and $\mathbf{R}_3$ (The dotted lines in figure 3.6).

We denote the strength of the transverse hop in relation to the others by λ, and set $a = t = 1$. The Hamiltonian for the diamond chain then becomes

$$\begin{aligned}\hat{H} =&(1+e^{ik})(\hat{a}^\dagger_{R_2}\hat{a}_{R_1} + \hat{a}^\dagger_{R_3}\hat{a}_{R_1}) + (1+e^{-ik})(\hat{a}^\dagger_{R_1}\hat{a}_{R_2} + \hat{a}^\dagger_{R_1}\hat{a}_{R_3}) \\ &+\lambda(\hat{a}^\dagger_{R_3}\hat{a}_{R_2} + \hat{a}^\dagger_{R_2}\hat{a}_{R_3}),\end{aligned} \tag{3.7}$$

and its matrix form is

$$\mathbf{H} = \begin{pmatrix} 0 & 1+e^{-ik} & 1+e^{-ik} \\ 1+e^{ik} & 0 & \lambda \\ 1+e^{ik} & \lambda & 0 \end{pmatrix}. \tag{3.8}$$

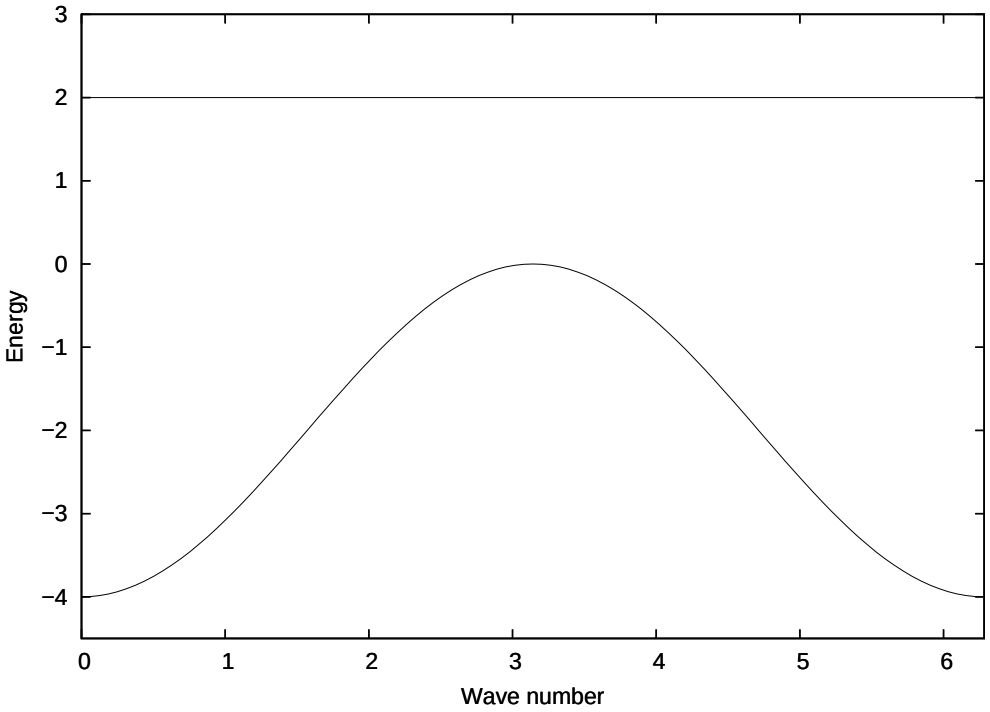

Figure 3.5: Energybands of a sawtooth chain (see figure 3.4)

The eigenenergies, seen plotted in figure 3.7, are

$$E_1 = -\frac{\lambda}{2} - \sqrt{8\cos^2\frac{k}{2} + \left(\frac{\lambda}{2}\right)^2}, \qquad E_2 = \lambda, \qquad E_3 = -\frac{\lambda}{2} + \sqrt{8\cos^2\frac{k}{2} + \left(\frac{\lambda}{2}\right)^2}, \tag{3.9}$$

and the energy eigenstates are

$$\begin{aligned}
\psi_1 &= N_1 \left((1 + e^{-ik}) \frac{\lambda - E_3}{4\cos^2\frac{k}{2} - \lambda E_3}, 1, 1 \right) \\
\psi_2 &= N_2 \left(0, -1, 1\right) \\
\psi_3 &= N_3 \left((1 + e^{-ik}) \frac{\lambda - E_1}{4\cos^2\frac{k}{2} - \lambda E_1}, 1, 1 \right).
\end{aligned}$$

In the diamond lattice the form of the flat-band state could be easily guessed. The neighboring unit cells are connected through site number one only, so a state with zero amplitude on it would be a good candidate for a flat-band state, if it could be made stationary. Because of the symmetry of

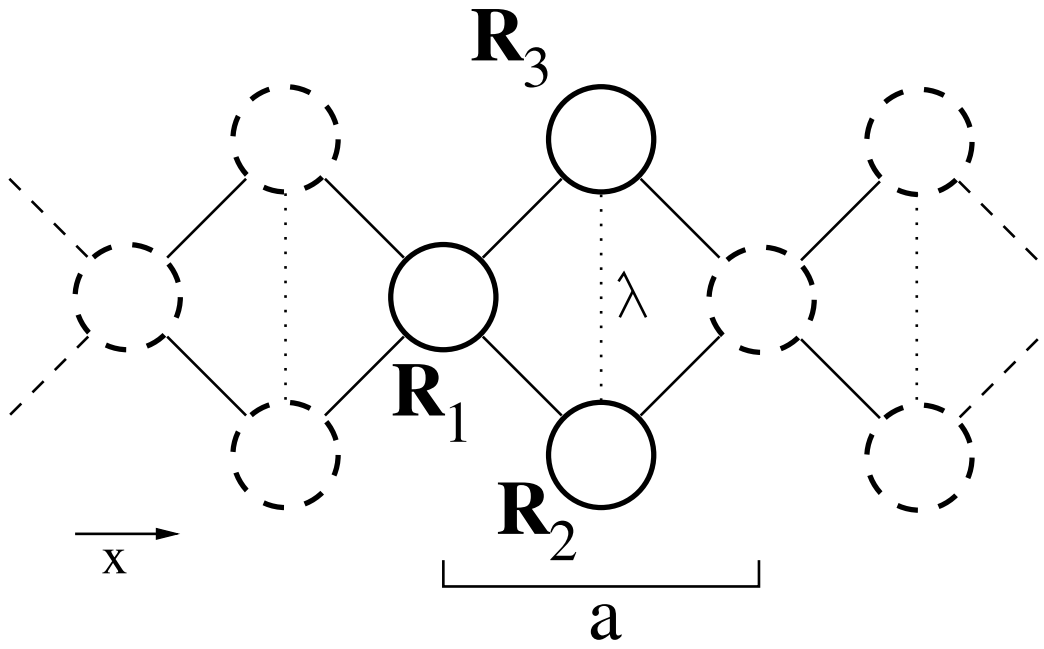

Figure 3.6: Structure of a diamond chain, and the numbering used for the sites of the primitive cell. λ denotes the relative strength of the transverse hopping terms.

the lattice, the stationarity can be achieved easily by setting the amplitudes on the sites two and three to have a 180 degree phase difference, in which case the amplitude flows to site one will pairwise cancel each other out. Changing the value of λ to differ from zero does not break the stationarity of such a state, but only accelerates the amplitude flow between the sites two and three. The i factor in the Hamiltonian causes an effective 90° phase shift in the amplitude flow, but since the phase difference between these sites is 180°, the resulting difference will still always be 90° and thus only cause rotation of the phases. The rotation speed thus scales linearly with the hopping term strength λ, and the energy of the state in turn scales linearly with the rotation speed (since the time dependence of the solutions to the Schrödinger equation in a stationary potential is always of the form e^{iEt}). This results in the λ dependent energy of the flat-band state ψ_2.

Similarly to the case of the rake chain, one can generate more flat-band lattices by extending the primitive cell of the diamond chain as in figure 3.3. We will again denote the eigenstates of an n-site linear chain by ϕ_i $(i = 1, \ldots, n)$. The resulting flat-band states of the infinite extended diamond

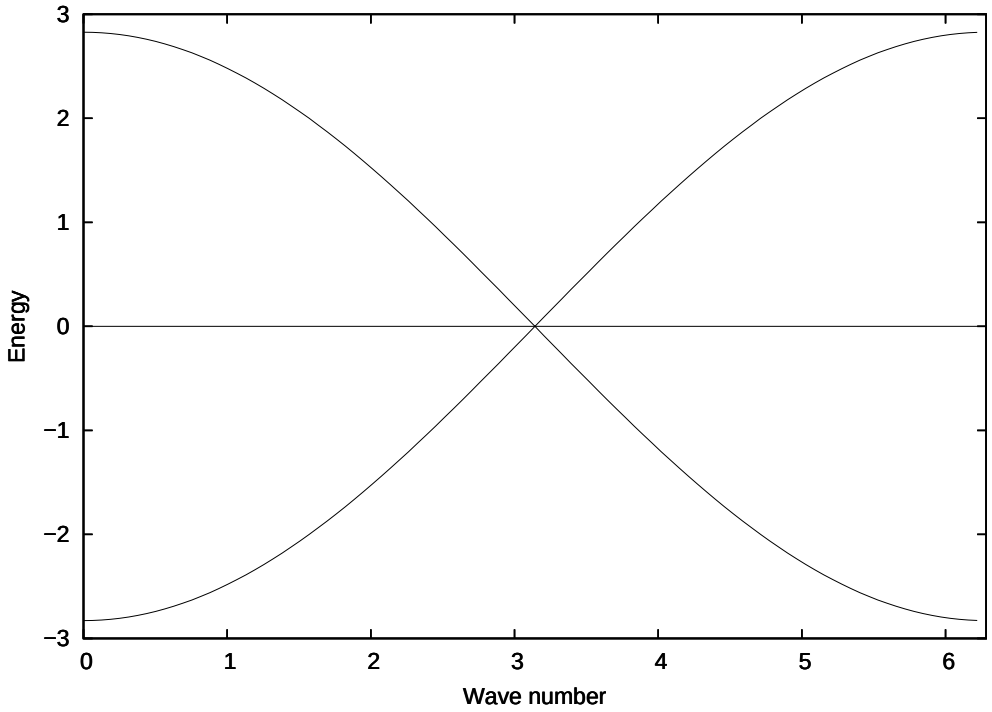

Figure 3.7: Energybands of a diamond chain for $\lambda = 0$ case (see figure 3.6)

chain will then be of the form

$$\psi_i = N_i \begin{pmatrix} 0 \\ -\phi_i \\ \phi_i \end{pmatrix}.$$

Chapter 4

Numerical Modeling

All of the numerical modeling for this thesis was done in Matlab.

The programs I developed support three types of one-dimensional chains. A linear chain, a sawtooth chain and a diamond-chain. In all of these chains the size of the unit cell can be freely chosen, and within the unit cell all the hopping terms and the site potentials can be individually set. This allows one to make, for example, a rake-chain by disabling some hops of the diamond-chain.

The programs can handle both bosons and fermions. There is also a separate option for bosons with infinite repulsive on-site interaction. This option approximates a very strong repulsive interaction, by allowing only one boson at a time to occupy any single lattice site. This is done by forming the systems basis only from the states which fulfill this condition. In large systems this results in a dramatically smaller basis, and correspondingly faster computation times. The infinitely repulsive bosons are then much like fermions, except that the states are symmetric, rather than antisymmetric, with respect to particle swaps. Spin is not taken into account, i.e. all the particles are assumed to be either spinless or spin-polarized.

For any of these chain type and particle type choices, one can use the programs to plot the energy bands, to solve and visualize the energy eigenstates, to compute and visualize the time-evolution of the system starting from any arbitrary state, and to compute the single particle state occupations corresponding to a multi-particle state.

4.1 Computing the Number of Basis States

The first problem was to compute the number of basis states for a system with a given unit cell and number of particles. The case of fermions is relatively

simple, and the formula (as already given in (2.26)) is

$$N_{states} = \frac{N_s!}{N_p!(N_s - N_p)!},$$

where N_s is the number of the lattice sites, and N_p is the number of the particles. This same formula works also in the case of infinitely repulsive bosons, since they similarly cannot share a site with another particle.

The case of interacting bosons is somewhat trickier. There is now no limit on the number particles per lattice site, and consequently there is no more any simple formula for acquiring the number of states. The question is: how many ways are there to distribute N_p particles into N_s lattice sites, when the particles are completely independent of each other, yet indistinguishable? My approach was to first go through the different numbers of stacks the particles may be divided to. This ranges from 1 to $\min(N_p, N_s)$. If we assume that there are N_{st} stacks, the following task is to figure out how many different ways there are to form these stacks. The question is then: how many ways are there to distribute $N_p - N_{st}$ particles into N_{st} lattice sites? We can subtract the number of stacks from the number of particles, since each stack always has at least one particle in it. We notice that this question is exactly the same as our original question, only with different (and smaller) parameters. Clearly this problem lends itself to a recursive solution. The algorithm I came up with is shown in the listing 4.1.

4.2 Forming the Basis States

The next task was to form all the basis states for a given system. These are all the possible ways in which the particles can be distributed into the lattice. They are represented as an $N_{states} \times N_{sites}$ matrix, whose each row corresponds to a basis state, and each column to a lattice site. The elements of this matrix have positive integer values, giving the number of particles in the lattice sites for each of the basis states. Each lattice site is here associated with a column index. This numbering of the sites can be chosen freely, but once set it must remain unchanged. The algorithms for forming the states matrix are given in the listing 4.2 for fermions (and for infinitely repulsive bosons), and in the listing 4.3 for bosons.

Listing 4.1: The algorithm for determining the number of basis states for a boson system

```
nSites = The number of sites in a unit cell
nParticles = The number of particles per unit cell


FUNCTION GetNumberOfStates(nParticles, nSites)
   nStates = 0
   FOR nStacks = 1 to minimum(nSites, nParticles)

      IF nParticles > nStacks
         nWaysToMakeStacks
               = GetNumberOfStates(nParticles - nStacks, nStacks);
      ELSE
         nWaysToMakeStacks = 1;
      END IF

      nWaysToOrderStacks = BinomialCoefficient(nSites, nStacks)

      nStates = nStates + nWaysToMakeStacks * nWaysToOrderStacks;

   END FOR
   RETURN nStates
END FUNCTION
```

Listing 4.2: The algorithm for forming the basis states matrix for fermions and infinitely repulsive bosons

```
nStates = The number of basis states in a unit cell
nSites = The number of sites in a unit cell
states = Matrix(nStates, nSites)
state = Vector(nSites)
stateNo = 1
FormStates(1, 1)


FUNCTION FormStates(particleNo, startIndex)
  FOR siteNo = startIndex to (nSites - nParticles + particleNo)

    state[SiteNo] = 1

    IF particleNo < nParticles
      FormStates(particleNo + 1, siteNo + 1)
    ELSE
      states[stateNo, :] = state
      stateNo++
    END IF

    state[siteNo] = 0

  END FOR
END FUNCTION
```

Listing 4.3: The algorithm for forming the basis states matrix for bosons

```
nStates = The number of basis states in a unit cell
nSites = The number of sites in a unit cell
nParticles = The number of particles per unit cell
states = Matrix(nStates, nSites)
state = Vector(nSites)
stateNo = 1
FormStates(1, 1)


FUNCTION FormStates(particleNo, startIndex)
  FOR siteNo = startIndex to nSites

    state[siteNo]++

    IF particleNo < nParticles
      FormStates(particleNo + 1, siteNo)
    ELSE
      states[stateNo, :] = state
      stateNo++
    END IF

    state(siteNo)--

  END FOR
END FUNCTION
```

4.3 Forming the Hamiltonian

The Hamiltonian is a $N_{states} \times N_{states}$ matrix, and its elements are the transition probabilities

$$\mathbf{H}_{ij} = \langle \psi_i | \hat{H} | \psi_j \rangle,$$

where ψ_n is the n:th basis state, and $\hat{H}$ is the Hubbard Hamiltonian (2.23). To compute the elements one needs to operate with the Hamiltonian to the right side basis state. This is relatively straightforward. Since the Hamiltonian is written in terms of creation and annihilation operators, one only needs to adjust the occupation numbers of the right side state accordingly. The resulting inner products between basis states can then be calculated using

$$\langle \psi_i | \psi_j \rangle = \delta_{ij},$$

i.e. the orthonormality of the basis.

In the case of fermions there exists an additional layer of complexity due to the anticommutativity of the creation and annihilation operators. Whereas for bosons one can freely operate with these operators without thought, for fermions one has to be careful to always maintain the correct order. What this order is does not matter, as long as it is consistently used for all the elements. I choose here to operate in the order of decreasing site number. Then, when operating with the Hamiltonian on a state, one first writes the right side state in terms of creation operators operating on a vacuum state, in the form

$$|n_1 n_2 \dots n_{N_s}\rangle = \prod_{i=1}^{N} (\hat{a}_i^\dagger)^{n_i} |0\rangle,$$

where $n_i \in \{0, 1\}$ are the site occupations. Operating with the terms of the Hamiltonian would then result in for example

$$\begin{aligned}
&- t\hat{a}_i^\dagger \hat{a}_j \left[(\hat{a}_1^\dagger)^{n_1} (\hat{a}_2^\dagger)^{n_2} \dots (\hat{a}_i^\dagger)^{n_i} \dots (\hat{a}_j^\dagger)^{n_j} \dots (\hat{a}_N^\dagger)^{n_N} |0\rangle \right] \\
&= - t(-1)^{\sum_{k=1}^{j-1} n_k} \hat{a}_i^\dagger \left[(\hat{a}_1^\dagger)^{n_1} (\hat{a}_2^\dagger)^{n_2} \dots (\hat{a}_i^\dagger)^{n_i} \dots \hat{a}_j (\hat{a}_j^\dagger)^{n_j} \dots (\hat{a}_N^\dagger)^{n_N} |0\rangle \right] \\
&= - t(-1)^{\sum_{k=1}^{j-1} n_k + \sum_{k=1}^{i-1} n_k} \left[(\hat{a}_1^\dagger)^{n_1} (\hat{a}_2^\dagger)^{n_2} \dots (\hat{a}_i^\dagger)^{n_i+1} \dots (\hat{a}_j^\dagger)^{n_j-1} \dots (\hat{a}_N^\dagger)^{n_N} |0\rangle \right],
\end{aligned} \tag{4.1}$$

assuming that $i < j$. If $j > i$ we start by flipping the operators, which creates one additional minus sign.

Due to the orthogonality of the basis, all the terms of the transition probability in which the right side state does not exactly match the left side state will go to zero. Because the Hamiltonian only contains pairs of

operators corresponding to a particle moving to a neighboring lattice site (as per the tight-binding approximation), a typical Hamiltonian will contain a very large number of zero valued elements. Even more so in the case of fermions, where a lot of the hops will result in a state that is not allowed by the Pauli exclusion principle. Therefore when it comes to storing and computing with the Hamiltonians, it is usually a good idea to treat them as sparse matrices.

4.4 Solving the Time-Evolution

An arbitrary state of the multi-particle system is a linear combination of the basis states

$$\Psi = \sum_{n=1}^{N_{states}} c_n \psi_n,$$

which is represented within Matlab as a column vector $\mathbf{v}$ with N_{states} elements. The time-evolution is computed by iterating on the initial state $\mathbf{v}(0)$ using a fourth order Runge-Kutta-method. The derivatives of the wave function are obtained from the Schrödinger equation

$$\frac{\partial \mathbf{v}(t)}{\partial t} = -i\mathbf{H}\mathbf{v},$$

where we have chosen a unit system in which $\hbar = 1$.

To obtain the evolved state $\mathbf{v}(\delta t)$ for a differential time interval δt, I start by computing the four derivatives for the fourth order Runge-Kutta-method in the following form

$$\begin{aligned}
d_1 &= -i\mathbf{H}\mathbf{v}(0) \\
d_2 &= -i\mathbf{H}\left(\mathbf{v}(0) + \frac{\delta t}{2} d_1\right) \\
d_3 &= -i\mathbf{H}\left(\mathbf{v}(0) + \frac{\delta t}{2} d_2\right) \\
d_4 &= -i\mathbf{H}\left(\mathbf{v}(0) + \delta t d_3\right).
\end{aligned}$$

I then compute the final state as

$$\mathbf{v}(\delta t) = v(0) + \frac{1}{6}\left(d_1 + 2d_2 + 2d_3 + d_4\right)\delta t.$$

After each of these time-steps the state vector $\mathbf{v}$ is normalized, in an attempt to slow down the inevitable deviation from the exact result.

The time-evolution could also be computed exactly, by solving all the energy eigenstates ψ_n of the system when $V = 0$, and expressing the initial state in that basis as

$$\psi_{init}(0) = \sum c_n \psi_n(0).$$

The form of the energy eigenstates after an arbitrary time of $\triangle t$ is obtainable simply by multiplying them with the corresponding phase terms $e^{iE_n \triangle t}$, where E_n is the energy of the state ψ_n. Thus

$$\psi_{init}(\triangle t) = \sum c_n \psi_n(\triangle t) = \sum c_n e^{iE_n \triangle t} \psi_n(0).$$

This method, while devoid of any accumulation of error, is relatively time-consuming, since it requires one to solve the entire eigensystem of the Hamiltonian. The Runge-Kutta method allowed much faster computation times, while still being easily accurate enough for my purposes.

4.5 Computing the Current

The current for a state ψ is computed simply by taking the expectation value of the current operator (2.55) with respect to ψ. The amount of computation needed can, however, be greatly lessened by appealing to certain symmetries of the ring.

For example in the case of the sawtooth lattice the currents through any of the node sites (sites corresponding to site 1 in picture 3.4) must obviously be the same. These currents further divide to the components going in the node from the left, and the ones leaving it towards right (or vice versa). These components must also have the same value, or else the occupation probability on that site would be changing over time. We can therefore take from the total current operator only the terms corresponding to hops from a certain node site of the ring to a certain direction, and in the end multiply this by the number of sites N_s to get the total current. Choosing as our node site the site number 1, we get

$$\begin{aligned}
\hat{C}_{sawtooth} &= iN_s \Big[t_{12} l_{12} e^{i\Phi l_{12}} \hat{a}_1^\dagger \hat{a}_2 + t_{21} l_{21} e^{i\Phi l_{21}} \hat{a}_2^\dagger \hat{a}_1 \\
&\qquad + \frac{1}{2} t_{13} l_{13} e^{i\Phi l_{13}} \hat{a}_1^\dagger \hat{a}_3 + \frac{1}{2} t_{31} l_{31} e^{i\Phi l_{31}} \hat{a}_3^\dagger \hat{a}_1 \Big] \\
&= iN_s \Big[t_{12} l_{12} (e^{i\Phi l_{12}} \hat{a}_1^\dagger \hat{a}_2 - e^{-i\Phi l_{12}} \hat{a}_2^\dagger \hat{a}_1) + \frac{1}{2} t_{13} l_{13} (e^{i\Phi l_{13}} \hat{a}_1^\dagger \hat{a}_3 - e^{-i\Phi l_{13}} \hat{a}_3^\dagger \hat{a}_1) \Big],
\end{aligned}$$

where we have substituted $e = 1$, $t_{nm} = t_{mn}$ and $l_{nm} = -l_{mn}$. Notice that we must take only a half of the terms corresponding to the hop from 1 to 3.

Otherwise multiplying by N_s would count these hops twice. Taking the site separation to be $a = 2$ (see figure 3.4), which leads to $l_{12} = \frac{1}{2\pi R}$, $l_{13} = \frac{1}{\pi R}$ and $N_s = 2\pi R$, we get

$$\hat{C}_{sawtooth} = i\Big[t_{12}(e^{i\Phi/2\pi R}\hat{a}_1^\dagger\hat{a}_2 - e^{-i\Phi/2\pi R}\hat{a}_2^\dagger\hat{a}_1) + t_{13}(e^{i\Phi/\pi R}\hat{a}_1^\dagger\hat{a}_3 - e^{-i\Phi/\pi R}\hat{a}_3^\dagger\hat{a}_1)\Big],$$

which is the form I use in my computations. The case of the diamond lattice is handled in an analogous way.

4.6 Computing single-particle state occupations

In order to determine whether the flat-band states of a system are populated or not, we would like to know which single particle states the particles of a certain multi-particle state are occupying. The occupation of any single-particle state φ_n can be expressed as

$$c_n = \langle\Psi|\hat{b}_n^\dagger\hat{b}_n|\Psi\rangle, \tag{4.2}$$

which is simply the expectation value of the number operator corresponding to the state φ_n. Here $|\Psi\rangle$ is a general multi-particle state. By expanding $|\Psi\rangle$ in the Fock-space Wannier-basis as

$$|\Psi\rangle = \sum_I A_I|\alpha_I\rangle$$

and expressing $\hat{b}$'s in terms of the Wannier-state creation/annihilation operators as

$$\hat{b}_n^\dagger = \sum_i B_{ni}^* a_i^\dagger, \qquad \hat{b}_n = \sum_i B_{ni} a_i,$$

we can write (4.2) as

$$c_n = \sum_{I,J}\sum_{i,j} A_I^* A_J B_{ni}^* B_{nj}\langle\alpha_I|\hat{a}_i^\dagger\hat{a}_j|\alpha_J\rangle,$$

which allows one to compute the occupations in a straightforward manner.

Chapter 5

Results

In this chapter I present the results from the numerical simulations I ran on multi-particle systems in the sawtooth and diamond chains. First I consider the case where the particles are initially confined in place by means of an external parabolic potential. I compute the time-evolution of the system once the external potential is removed, and note the effect of occupied flat-band states on the results. Next I compute the currents caused by magnetic flux through rings formed by the chains, and plot them as functions of the particle number. Again I note the connection between these results and the band structure of the chain.

5.1 Time-Evolution of a Confined State

The initial confined state ψ_{init} is computed by first adding to the Hubbard Hamiltonian (2.23) a parabolic potential term

$$V_j = V \sum_i (x_i - x_j)^2 \hat{n}_i, \tag{5.1}$$

where V controls the strength of the confinement and j is the site it is centered on. ψ_{init} is the ground state of this Hamiltonian. The time-evolution of the system is then computed as per section 4.4 starting from ψ_{init} and using a Hamiltonian with no external potential term. In all of the computations shown here a value of $V = 10$ was used.

All of the time-developments were computed over 500 steps with a step length of $\delta t = 0.005$.

5.1.1 Sawtooth Chain

Figure 5.1 shows the time developments for confined states of 1 to 4 fermions in the sawtooth chain. It is seen that as more particles are added into the system, the wave function becomes more and more stationary with only a certain part of it dispersing once the confinement is removed. This is the behavior one would except to see when the non-mobile flat-band states become increasingly occupied.

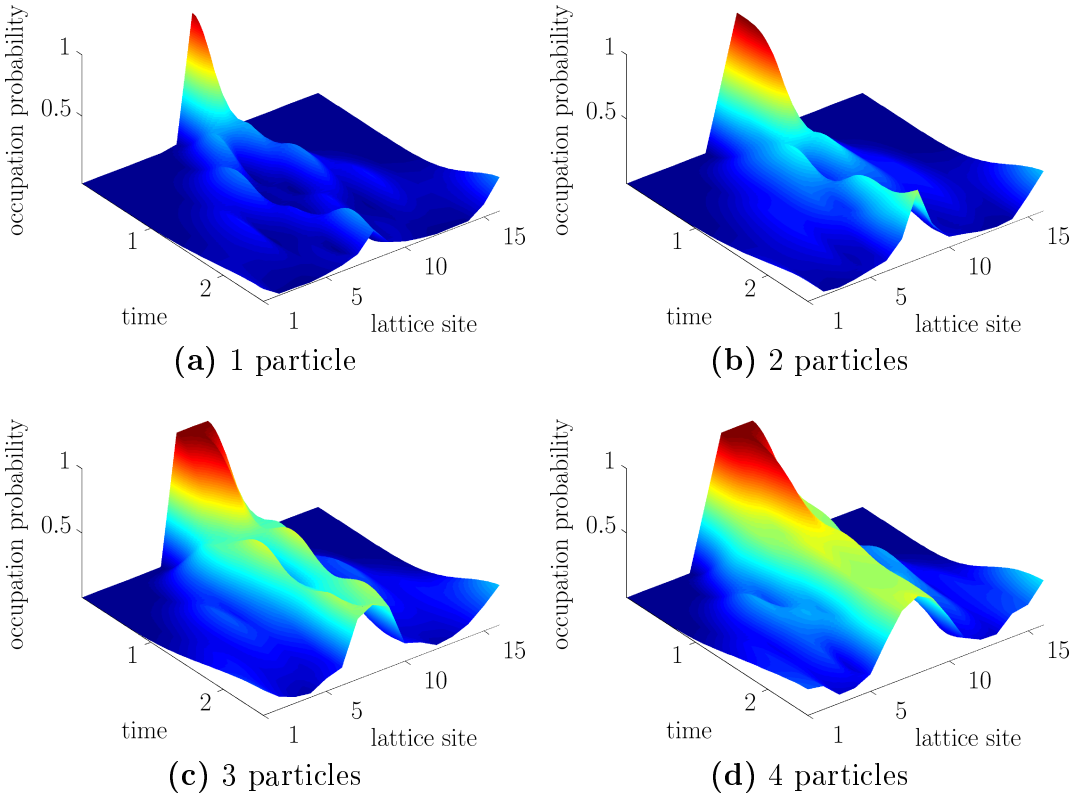

(a) 1 particle **(b)** 2 particles

(c) 3 particles **(d)** 4 particles

Figure 5.1: Time developments of confined fermionic states of 1 to 4 particles in a sawtooth chain of 16 sites. Here $j = 8$.

The connection is seen more clearly in figure 5.2 where a similar time development computation is shown for 1 and 2 bosons, along with graphs showing the projections of the initial wave function to the single particle states of the system (see section 4.6). Here the sign of the baseline hopping term of the sawtooth chain has been flipped, which makes the flat-band states the ground states of the system (without this it proved to be difficult to get the bosons into the flat-band states at all). The lessened spreading of

the wave function corresponds clearly with the increased occupation of the flat-band states.

5.1.2 Diamond Chain

Figure 5.3 shows the time-development of one and two particle confined states of both fermions and bosons in a diamond chain. It is seen that in the case of a single particle there is no difference between a bosonic and a fermionic state. This is to be expected. Since the only difference between the particle types is the behavior of the wave function under the swapping of two particles, a single particle does not care whether it is a boson or a fermion.

When the second particle is added, however, the results diverge. In the case of fermions the second particle seems to go to a flat-band state. The occupation probability in the two sites at the center of the confining potential falls quickly to about a half of its initial value, but then remains approximately constant for the rest of the simulation. Conversely for bosons the evolution of a two particle state is pretty much identical to that of the single particle state, with the wave function dispersing in its entirety.

When the flat-band is moved below the other bands by setting $\lambda = -2.1$ (see equation (3.9)) the situation changes. The first particle inserted into the system now goes completely to a flat-band state as seen in figure 5.4. The case of two-particle states is similar to figure 5.3 in that the bosonic state is decidedly more eager to spread out than the fermionic state which is still to large a degree stationary.

5.2 Currents in a Ring

I computed the current flow in sawtooth and diamond rings of 12 lattice sites. I give the results here for particle numbers from 1 to 11, and for values of the magnetic flux Φ' (see equation (2.49)) going from 0 to 0.5 in 0.1 increments (the last step is actually done with $\Phi' = 0.4999$ to avoid problems created by a higher degeneracy of the states at $\Phi' = 0.5$). This range of fluxes is sufficient, since the currents are antisymmetric around $\Phi' = 0.5$, falling back to zero for $\Phi' = 1$, and then repeat periodically for larger values of Φ'. Currents were always computed for the ground state of the system, and the results are given in units in which $e = 1$.

5.2.1 Sawtooth Ring

For the sawtooth ring I computed the currents both with the normal hopping term configuration (see figure 3.5) and with the sign of the hopping term along the base flipped (which flips the signs of the eigenenergies, thus swapping the energy bands). The respective results are given for bosons in figure 5.5 and figure 5.6, and for fermions in figure 5.7 and figure 5.8.

The occupation of the flat band states is clearly visible in the figures. Particles on the flat band states do not move (as seen from equation (2.37)), and therefore do not contribute to the current. Thus if a particle is added into a flat-band state, the total current does not change.

If a particle is added into a non-flat-band state, the change in the current depends on the slope of the energy band at that point. Typically for these lattices, the slopes of the wave like energy bands are alternatively positive and negative. For fermions, which due to the Pauli exclusion principle simply fill the single particle states in order, this alternating of the slope sign manifests as a zigzag pattern seen for example in picture 5.7.

In the bosonic case the currents are symmetric with respect to the particle number. This phenomenon can be understood by considering the same system in terms of holes instead of particles. We can make the substitution

$$\hat{a}_i^\dagger = \hat{b}_i, \qquad \hat{a}_i = \hat{b}_i^\dagger,$$

where $\hat{b}_i^\dagger$ and $\hat{b}_i$ are the creation and annihilation operators for a hole. Because for bosons these operators commute, it holds that $\hat{a}_i^\dagger \hat{a}_i = \hat{b}_i^\dagger \hat{b}_i$, and therefore the Hamiltonian of the hole system is identical to that of the particle system. A bosonic system with n particles is thus completely equivalent to a system with n holes, and the currents also must follow this symmetry.

5.2.2 Diamond Ring

For the diamond ring I computed the currents using two different values for the transverse hop parameter λ (see equation (3.7)), $\lambda = 0$ (see figure 3.7) and $\lambda = -2.1$. The latter moves the flat-band from the center to below the other bands, and thus makes the flat-band states the ground states of the system. The respective results are given for bosons in figure 5.9 and figure 5.10, and for fermions in figure 5.11 and figure 5.12.

As an example, the energy band diagram corresponding to figure 5.11 is given in figure 5.13. Changes of the current with respect to the increasing particle number can be understood by considering the bands being occupied in succession starting from the bottom. The alternating slopes of the wave

like bands create the zigzag pattern, and the four degenerate flat-bands create the plateau in the middle.

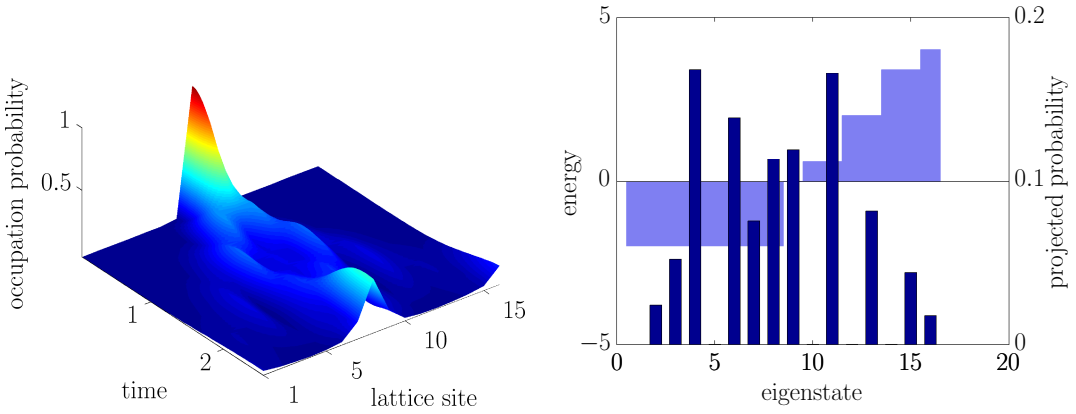

(a) 1 particle

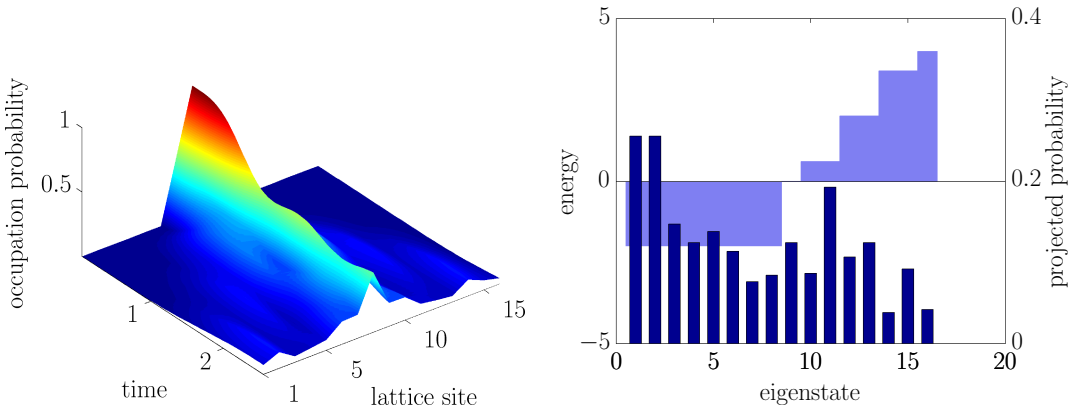

(b) 2 particles

Figure 5.2: Time developments of confined bosonic states with 1 and 2 particles in a sawtooth chain of 16 sites. Here $j = 8$ and the baseline hopping term sign has been flipped. On the right side are shown the projections of the initial states into the single particle basis, with the energies of the single particle states in the background. The flat-band states are recognizable by their high degeneracy

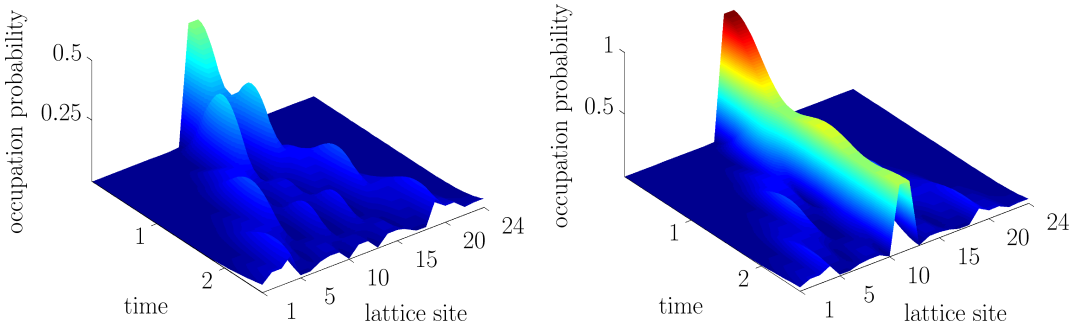

(a) 1 fermion

(b) 2 fermions

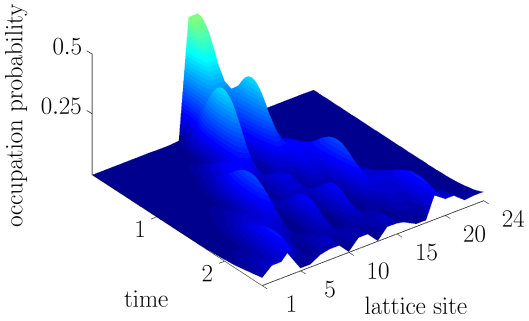

(c) 1 boson

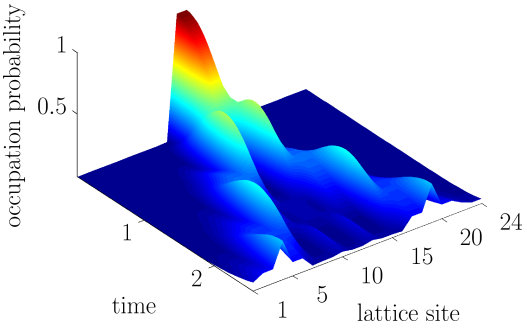

(d) 2 bosons

Figure 5.3: Time developments of confined fermionic and bosonic states with 1 and 2 particles in a diamond chain of 24 sites. Here $j = 12$ and $\lambda = 0$.

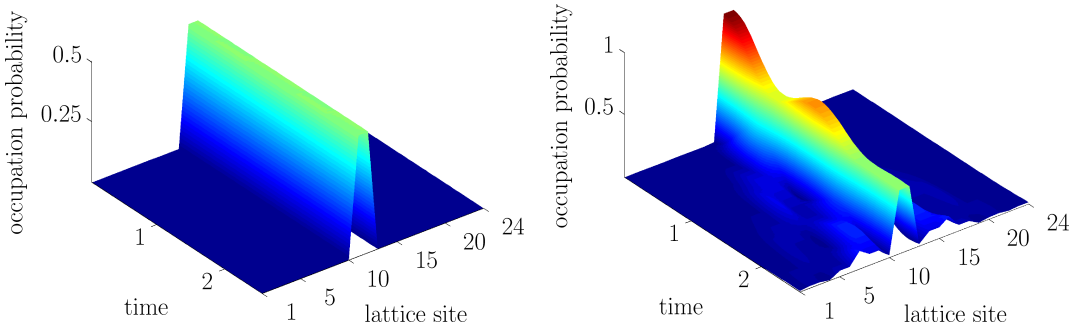

(a) 1 fermion

(b) 2 fermions

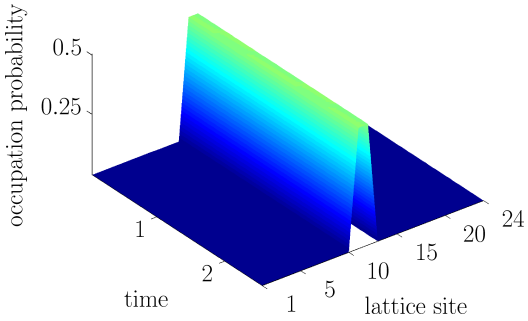

(c) 1 boson

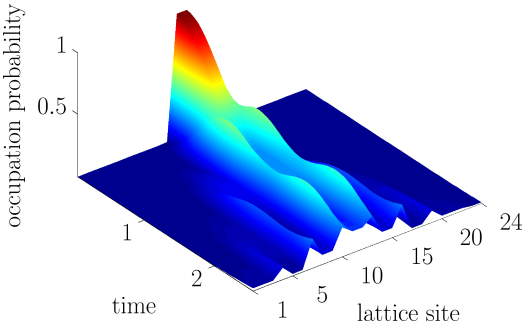

(d) 2 bosons

Figure 5.4: Time developments of confined fermionic and bosonic states with 1 and 2 particles in a diamond chain of 24 sites. Here $j = 12$ and $\lambda = -2.1$.

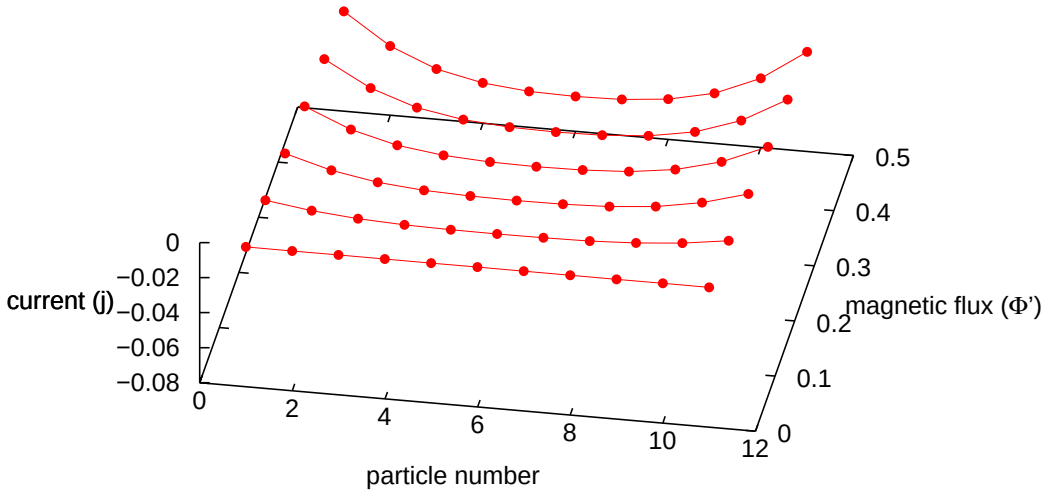

Figure 5.5: The current for infinitely repulsive bosons in a sawtooth ring of 12 sites as a function of the particle number and the magnetic flux (Φ') through the ring.

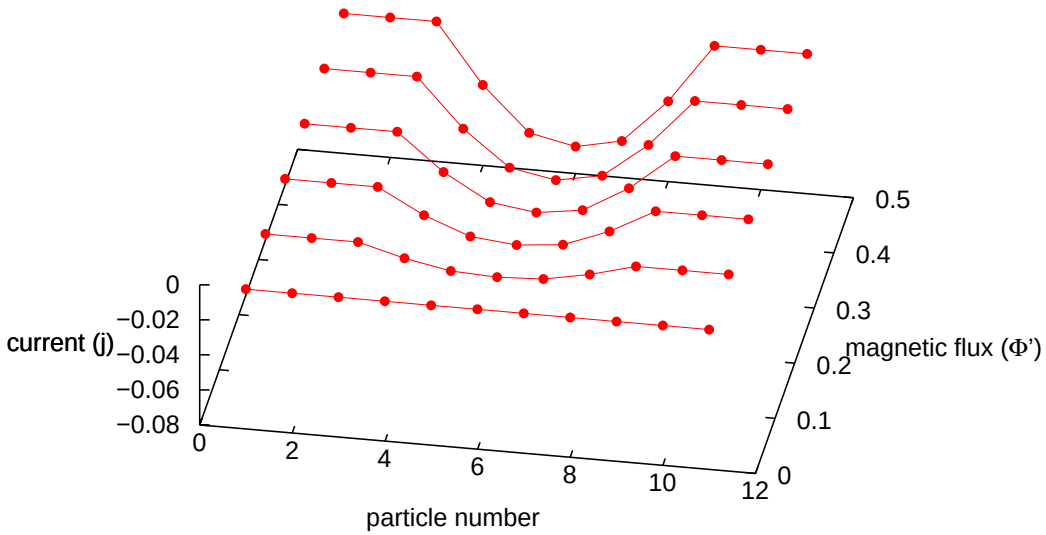

Figure 5.6: The current for infinitely repulsive bosons in a sawtooth ring of 12 sites as a function of the particle number and the magnetic flux (Φ') through the ring. Here the sign of the baseline hopping term has been flipped, which makes the flat bands the lowest energy bands in the system.

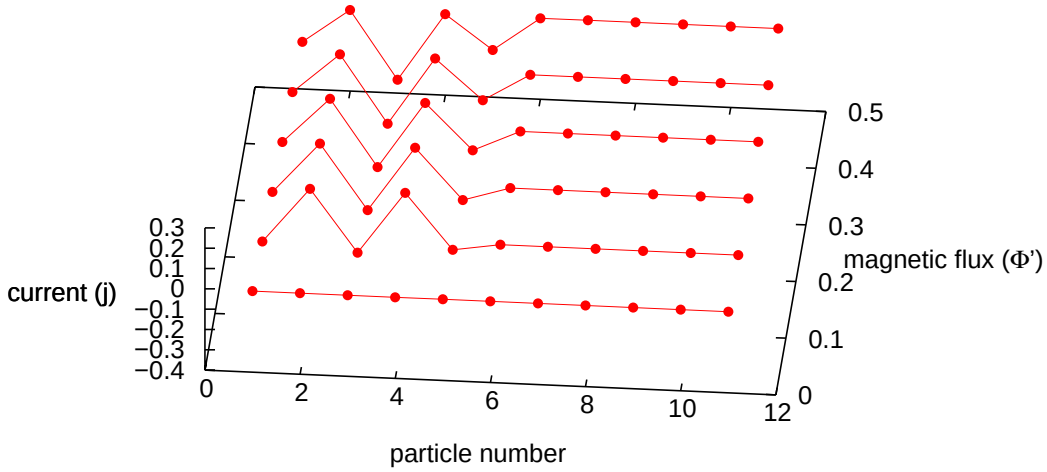

Figure 5.7: The current for fermions in a sawtooth ring of 12 sites as a function of the particle number and the magnetic flux (Φ') through the ring.

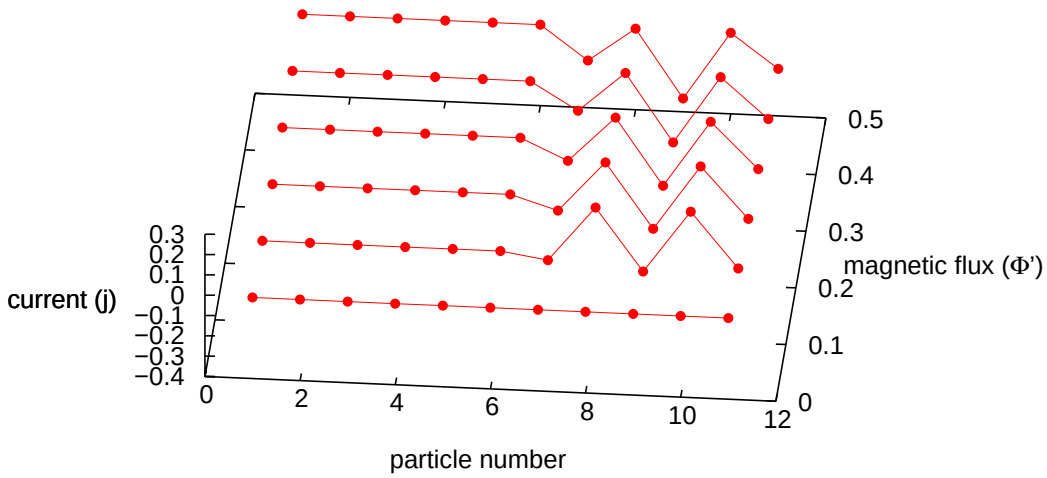

Figure 5.8: The current for fermions in a sawtooth ring of 12 sites as a function of the particle number and the magnetic flux (Φ') through the ring. Here the sign of the baseline hopping term has been flipped, which makes the flat bands the lowest energy bands in the system.

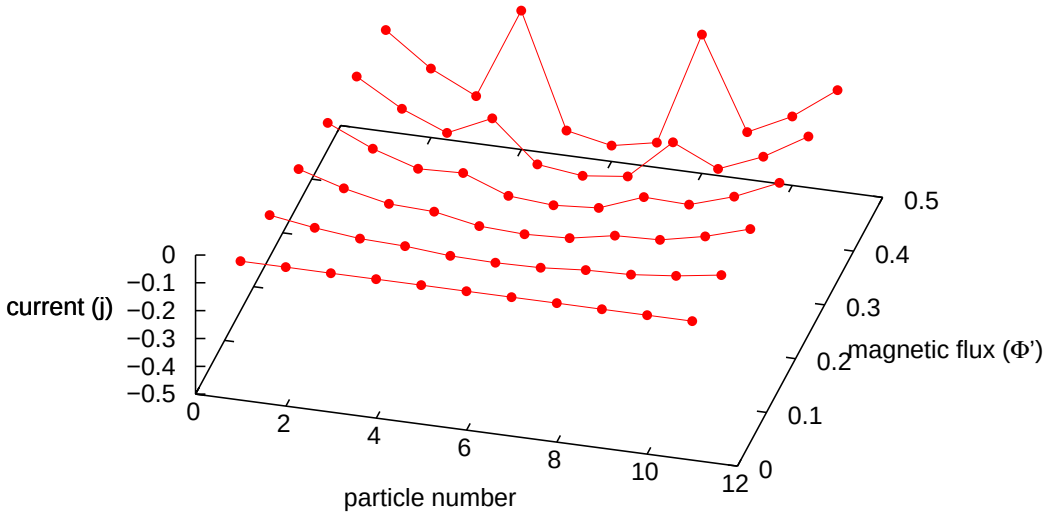

Figure 5.9: The current for infinitely repulsive bosons in a diamond ring of 12 sites as a function of the particle number and the magnetic flux (Φ') through the ring.

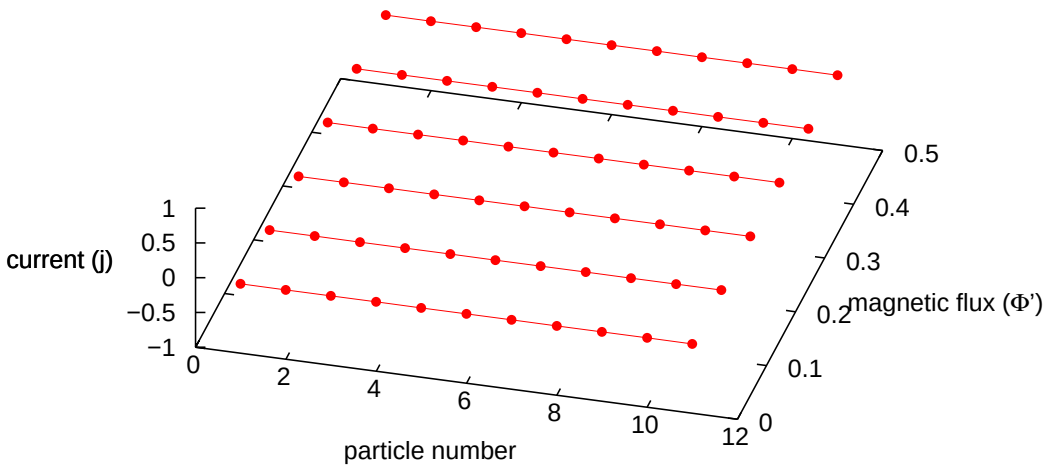

Figure 5.10: The current for infinitely repulsive bosons in a diamond ring of 12 sites as a function of the particle number and the magnetic flux (Φ') through the ring. Here the transverse hopping term has been set to -2.1, which makes the flat bands the lowest energy bands in the system.

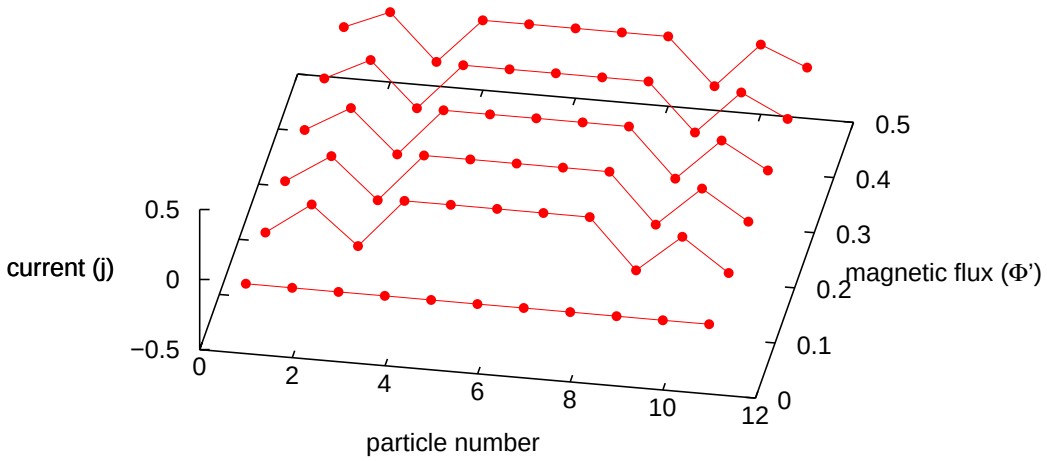

Figure 5.11: The current for fermions in a diamond ring of 12 sites as a function of the particle number and the magnetic flux (Φ') through the ring.

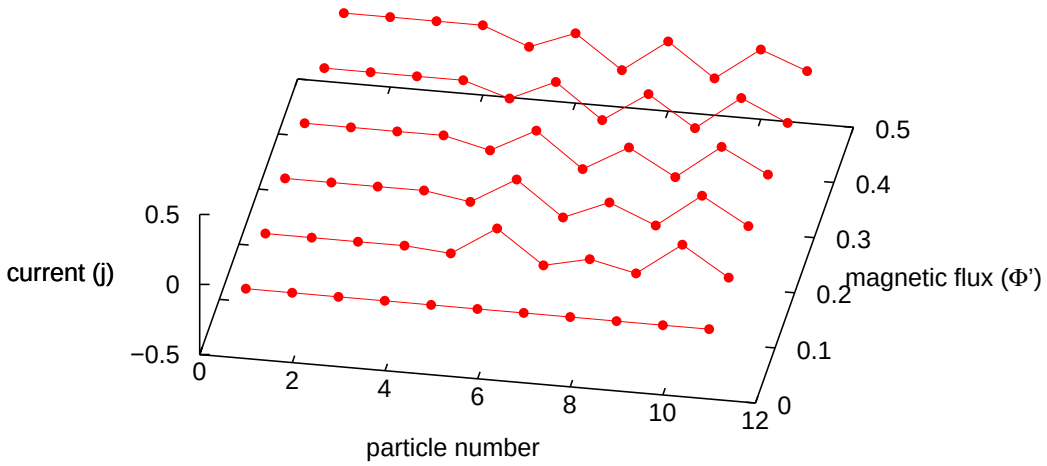

Figure 5.12: The current for fermions in a diamond ring of 12 sites as a function of the particle number and the magnetic flux (Φ') through the ring. Here the transverse hopping term has been set to -2.1, which makes the flat bands the lowest energy bands in the system.

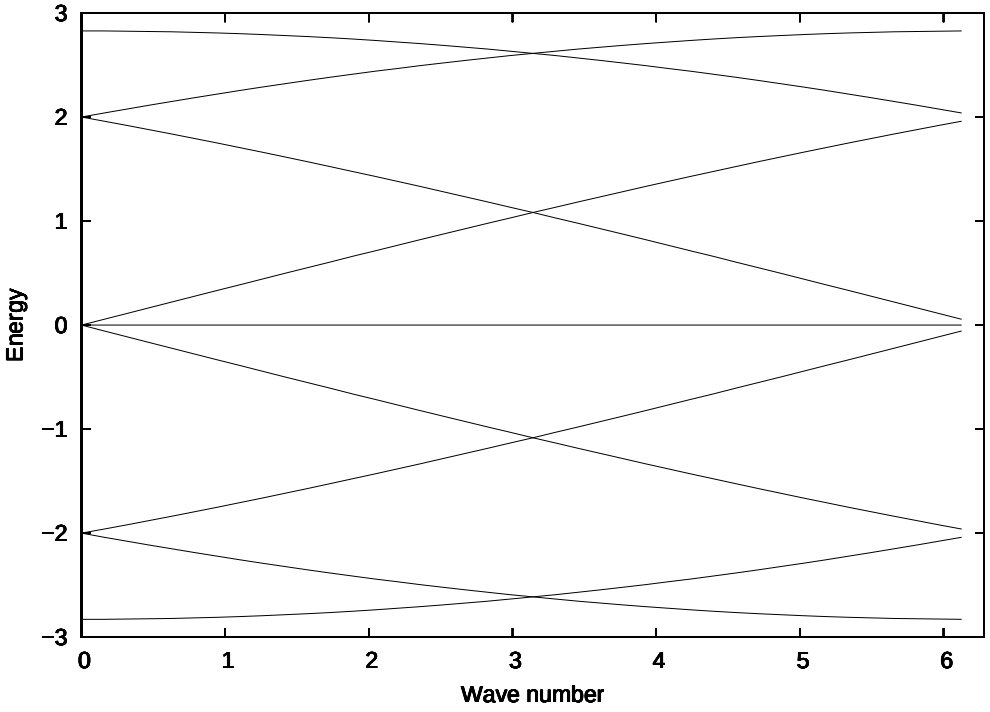

Figure 5.13: The energy bands of a diamond chain with a 12 site unit cell. The flat-band is four times degenerate.

Chapter 6

Conclusions

I set out to study the effects caused by the existence of flat-bands in one dimensional chains. The results I obtained show many clear examples of these effects, and they are mostly in line with what one could have predicted beforehand from the fact that the particles on flat-band states have a zero group velocity. The occupation of the flat-band states is manifested as a stationary nature of the wave function (seen for example in figure 5.2), and as suppression of the current in a ring (seen for example in figure 5.8).

Regarding the computations of the time evolutions of confined states, in the case of fermions in a sawtooth chain (figure 5.1) my results show a clearly decreasing amount of dispersion of the wave function as more particles are loaded in to the chain. This was an expected result, as the flat-band is the higher of the two bands and therefore will only be used after the Pauli repulsion prevents the use of the states of the lower band. This interpretation is confirmed by the fact that bosons in a similar set up were far more reluctant to occupy the flat-band states. In the case of bosons I needed to modify the hopping terms in such a way as to make the flat-band the lowest energy band. After this operation the bosons started to show clear signs of flat-band occupation (see figure 5.2).

In the case of the diamond lattice, the results were similar. If the flat-band was situated symmetrically between the other two bands (figure 5.3), the bosons would not go into it, whereas for fermions already two particles in a 24 site unit cell were enough for significant flat-band occupation. If the flat-band was moved below the other bands (figure 5.4), the first particle, whether a boson or a fermion, went completely on a flat-band state. The second particle, however, made a difference. In the case of fermions it looks like the second particle went on a non-flat-band state, leaving the first one still stuck on the flat-band, while for bosons the second particle disturbed the first one causing the total wave function to disperse much more completely. This

can also be explained through the Pauli principle (which is the only option, since after neglecting the spin it is the only difference between bosons and fermions), which forces the fermions on mutually orthogonal states and thus makes them essentially independent.

Note that in all the cases the evolution of a single fermion is exactly similar to that of a single boson. This is natural, since the Pauli repulsion follows from the symmetry properties of the wave function under the swapping of two particles. A single particle, therefore, does not care whether it is a boson or a fermion.

The results of the current computations for fermions are easy to interpret, as they correspond clearly to the energy band diagrams of the respective rings. They confirm that as fermions are added to a system, they sequentially occupy the single particle states, without disturbing each other. Each particle changes the current according to the group velocity corresponding to its state, and thus the degenerate flat-bands cause flat stretches of constant current to show up. The bosonic case is more difficult to analyze, as the multi-particle ground states are much more complicated combinations of the single-particle states. Still, for bosons too, the occupation of the flat-band is in some cases clearly visible (see figure 5.6). Interestingly the plots for bosons in the diamond lattice show sudden spikes in the current (figure 5.9), or no current at all (figure 5.10). Explaining these would require further studies into the nature of the corresponding multi-particle wave functions.

These results were computed using the Hubbard model, and as such they are applicable to any optical lattice system built in such a way as to realize that model. Only further simplifications made are the assumption of using either a spinless or a spin polarized gas, and the assumption of a large gap between the first and second bound states of the potential wells. Both of these conditions can be readily fulfilled in an experiment.

While the current computations are exact in the context of the model, the time-development computations obviously contain some error due to the use of an approximate Runge-Kutta method for solving the Schrödinger equation. However, the limiting factor on the time-scale of these computations is not the accumulation of error, but rather the small size of the unit cell used. The fringes of the wave function relatively quickly reach the edges of the cell, after which point the results no longer describe an infinitely long chain. Because of this I have not devoted much effort into trying to quantify the errors, but rather have just made the time-step short enough that the results no longer visibly depend on it. On the whole, therefore, there should be no appreciable error of numerical origin in any of the results given in this thesis.

The downside of doing an exact multi-particle treatment as is done here, is that the number of states in the system, and thus the dimension of the Hamil-

tonian, increases extremely quickly when the number of sites or particles is increased (see equation (2.26)). This puts a strict limit on the maximum size of a system that can be dealt with in a reasonable time frame. There is no easy way around this. As is shown in [22], a mean field calculation would not give reliable results in this kind of a strongly correlated case.

References

[1] V. S. Letokhov, *Narrowing of the Doppler Width in a Standing Wave*, JETP Letters **7**, 272 (1968)

[2] C. Salomon, J. Dalibard, A. Aspect, H. Metcalf, and C. Cohen-Tannoudji, *Channeling atoms in a laser standing wave*, Phys. Rev. Lett. **59**, 1659 (1987)

[3] M. Lewenstein, A. Sanpera, V. Ahufinger, B. Damski, A. Sen De and U. Sen, *Ultracold Atomic Gases in Optical Lattices: Mimicking Condensed Matter Physics and Beyond*, Adv. Phys. **56**, 243 (2007)

[4] O. Morsch and E. Arimondo, *Ultracold atoms and Bose-Einstein condensates in optical lattices*, in T. Dauxois, S. Ruffo, E. Arimondo and M. Wilkens (Editors), "Dynamics and Thermodynamics of Systems With Long Range Interactions", (Springer, Berlin, 2002) p. 312, arXiv:cond-mat/0209034v1

[5] P. S. Jessen, I. H. Deutsch, R. Stock, *Quantum Information Processing with Trapped Neutral Atoms*. Quant. Inf. Proc. **3**, 91 (2004)

[6] C. J. Pethick and H. Smith, *Bose-Einstein Condensation in Dilute Gases*, Second Edition (Cambridge University Press, Cambridge, 2008)

[7] I. Bloch, *Ultracold Quantum Gases in Optical Lattices*, Nature Physics **1**, 23 (2005)

[8] F. Bloch, *Über die Quantenmechanik der Elektronen in Kristallgittern*, Z. Physik **52**, 555 (1928)

[9] C. Chin, R. Grimm, P. Julienne and E. Tiesinga, *Feshbach Resonances in Ultracold Gases*, Rev. Mod. Phys. **82**, 1225 (2010)

[10] N.W. Ashcroft and N.D. Mermin, *Solid State Physics* (Saunders College Publishing, Philadelphia, 1976)

[11] H. Ibach and H. Luth, *Solid State Physics*, Second Edition (Springer, Berlin, 1996)

[12] J. Hubbard, *Electron Correlations in Narrow Energy Bands*, Proc. R. Soc. Lond. A **276**, 238 (1963)

[13] E. H. Lieb and F. Y. Wu, *Absence of Mott Transition in an Exact Solution of the Short-Range, One-Band Model in One Dimension* Phys. Rev. Lett. **20**, 1445 (1968)

[14] P. W. Anderson, *Superconductivity in High Tc Cuprates: The Cause is No Longer A Mystery* in T. Claeson and P. Delsing (Editors), "Condensation and Coherence in Condensed Matter, Proc. of the Nobel Jubilee Symposium, Göteborg 2001", (Physica Scripta/The Royal Academy of Sciences/World Scientific, Singapore, 2003)

[15] D. Jaksch, C. Bruder, J. I. Cirac, C. W. Gardiner, and P. Zoller, *Cold Bosonic Atoms in Optical Lattices*, Phys. Rev. Lett. **81**, 3108 (1998)

[16] J.M. Ziman, *Electrons and Phonons*, Oxford Classics Series version (Oxford University Press, Oxford, 2001)

[17] W. Kohn, *Analytic Properties of Bloch Waves and Wannier Functions*, Phys. Rev. **115**, 809 (1959)

[18] L. D. Landau and E. M. Lifshitz *Quantum Mechanics: Non-Relativistic Theory*, Second Edition (Pergamon Press, Oxford, 1965)

[19] F. H. L. Essler, H. Frahm, F. Göhmann, A. Klümper and V.E. Korepin, *The One-Dimensional Hubbard Model*, (Cambridge University Press, Cambridge, 2005)

[20] S. Deng, A. Simon and J. Köhler, *The Origin of a Flat Band*, J. Solid State Chem. **176**, 412 (2003)

[21] L. Amico, A. Osterloh and F. Cataliotti, *Quantum Many Particle Systems in Ring-Shaped Optical Lattices*, Phys. Rev. Lett. **95**, 063201 (2005)

[22] V. Apaja, M. Hyrkäs and M. Manninen, *Flat Bands, Dirac Cones and Atom Dynamics in an Optical Lattice*, Phys. Rev. A **82**, 041402(R) (2010)